Electronic Supplementary Information (ESI)

Conformer-dependent self-assembly metallacycles with photo-reversible response

Mengqi Li,[‡a] Li-Jun Chen,[‡b] Zhipeng Zhang,[a] Qianfu Luo,[a] Hai-Bo Yang*[b], He Tian[a] and Wei-Hong Zhu*[a]

[a]*Key Laboratory for Advanced Materials and Institute of Fine Chemicals, Shanghai Key Laboratory of Functional Materials Chemistry, Joint International Research Laboratory of Precision Chemistry and Molecular Engineering, Feringa Nobel Prize Scientist Joint Research Center, School of Chemistry and Molecular Engineering, East China University of Science and Technology, Shanghai 200237, China. E-mail: whzhu@ecust.edu.cn*
[b]*Shanghai Key Laboratory of Green Chemistry and Chemical Processes, Chang-Kung Chuang Institute, School of Chemistry and Molecular Engineering, East China Normal University, Shanghai 200062, China. E-mail: hbyang@chem.ecnu.edu.cn*

Contents

1. Experimental section

1.1 General

All starting reagents were used without further treatment. 4-Pyridineboronic acid was purchased from Adamas Reagent Co., Ltd. *ap*-**PY**, *p*-**PY**, *c*-**PY**, *ap*-**[3+3]**, *c*-**[3+3]**[1] and 180° or 120° di-Pt (II) acceptors **1** or **2**[2,3] were prepared according to the established methods. Solvents used were analytical grade without further treatment, except those for recrystallization and optical tests, which were purified by distillation. TLC analysis was performed on silica-gel plates, and column chromatography was conducted using silica-gel column packages purchased from Qingdao Haiyang Chemical (China). NMR spectra were recorded on Bruker AM-400 spectrometers with tetramethylsilane (TMS) as an internal reference, $CDCl_3$, CD_2Cl_2, Acetone-d_6, methanol-d_4 and DMSO-d_6 as solvents. High resolution mass (HRMS) spectra were recorded on a Waters LCT Premier XE spectrometer with methanol or acetonitrile as solvents. UV/Vis spectra were recorded on Agilent Cary 60 (1 cm quartz cell) at 25 ºC. Fluorescence spectra were recorded using HORIBA Fluoromax 4. Fluorescence lifetimes were measured on an Edinburgh Lifespec-PS spectrofluorometer (FL920).

The photochromic reaction was induced *in situ* by continuous irradiation using an Hg/Xe lamp (Hamamatsu, LC8 Lightningcure, 200 W) equipped with a narrow band interference filter (Shenyang HB optical Technology) for λ_{irr} = 302 ± 20 nm, a broad band interference filters (Shenyang HB optical Technology) for λ_{irr} > 480 nm. The photochromic reaction quantum yields were evaluated by the standard procedures using BTF_6 as the reference for photocyclization and cycloreversion.[4] The rates of isomerization in the initial stage of the reaction (0-3%) were compared with references, whose $\Phi_{o\text{-}c}$ (35%) and $\Phi_{c\text{-}o}$ (35%) in hexane. It brought forth 3% uncertainties on the calculations of quantum yields. The fluorescence quantum yields (Φ_F) were measured using anthracene in EtOH (27%) as reference.[5]

1.2. Self-assembly and characterization of metallacycles

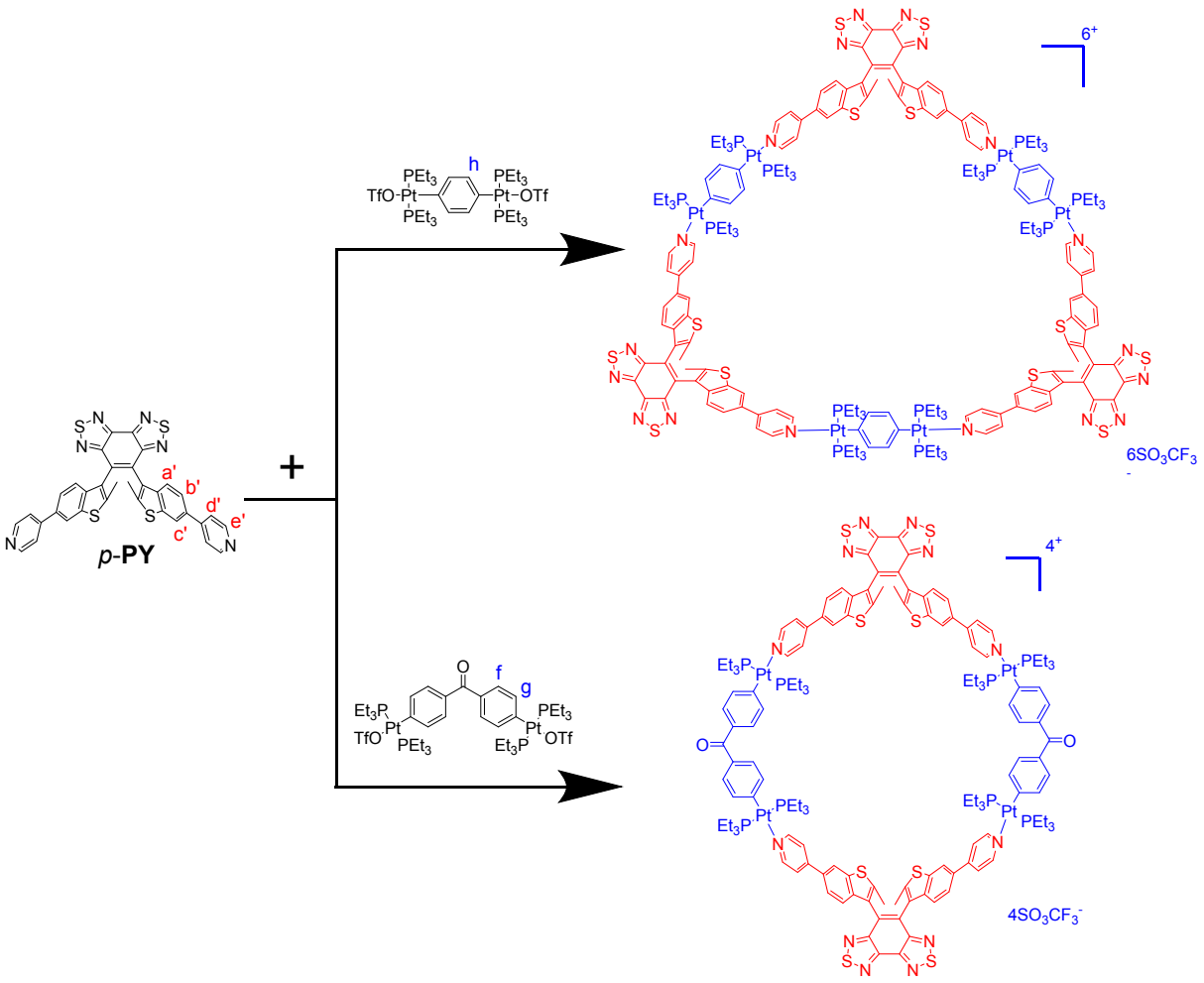

Scheme S1 Self-assembly of supramolecular hexagon *p*-**[2+2]** and *p*-**[3+3]** from parallel conformer ligand *p*-**PY** and di-platinum acceptor **1** and **2**.

Synthesis of the *p*-[3+3] Triangle: The dipyridyl donor ligand *c*-**PY** (1.96 mg, 3.06 μmol) and the organoplatinum 180° acceptor **2** (3.78 mg, 3.06 μmol) were weighed accurately into a glass vial away from light. To the vial was added 0.6 mL of CD_2Cl_2 solvent, and the reaction solution was then stirred in the dark place at room temperature for 5 h to yield a homogeneous solution. The solution was then transferred into the NMR tube to collect ^1H and ^{31}P NMR spectra. Light yellow solid product was obtained by removing the solvent under vacuum. Yield: 5.74 mg, > 99%. ^1H NMR (CD_2Cl_2, 400 MHz, ppm): δ 0.99-1.02 (m, 108 H, –$PCH_2C\mathbf{H_3}$), 1.25 (s, 72 H, –$PC\mathbf{H_2}CH_3$), 2.32 (s, 18 H, -CH_3), 6.95 (s, 12 H, phenyl-H), 7.27-7.36 (m, 6 H, benzothiophene-H), 7.44-7.55 (m, 6 H, benzothiophene-H), 7.87 (d, J = 4.4 Hz, 12 H, pyridine-H), 8.13 (s, 6 H, benzothiophene-H), 8.56 (s, 12 H, pyridine-H). ^{31}P NMR (CD_2Cl_2, 161.9 MHz, ppm): δ 12.85 ($J_{Pt\text{-}P}$ = 2726.4 Hz). MS (ESI-MS): *m/z* calcd for [*p*-[**3+3**] - 5OTf$^-$]$^{5+}$ 977.42, found 977.50; [*p*-[**3+3**] - 4OTf$^-$]$^{4+}$ 1258.27, found 1258.36; [*p*-[**3+3**] - 3OTf$^-$]$^{3+}$ 1728.01, found 1728.11.

Synthesis of the *p*-[2+2] Rhomboid: The dipyridyl donor ligand *p*-**PY** (1.71 mg, 2.67 μmol) and the organoplatinum 120° acceptor **1** (3.58 mg, 2.67 μmol) were weighed accurately into a glass vial away from light. To the vial was added 0.6 mL of CD_2Cl_2 solvent, and the reaction solution was then stirred in the dark place at room temperature for 5 h to yield a homogeneous solution. The solution was then transferred into the NMR tube to collect ^1H and ^{31}P NMR spectra. Light yellow solid product was obtained by removing the solvent under vacuum. Yield: 5.29 mg, > 99%. ^1H NMR (CD_2Cl_2, 400 MHz, ppm): δ 1.01-1.07 (m, 72 H, –$PCH_2C\mathbf{H_3}$), 1.27 (s, 48 H, –$PC\mathbf{H_2}CH_3$), 2.32 (d, 12 H, -CH_3), 7.27-7.32 (m, 4 H, benzothiophene-H), 7.41-

7.51 (m, 20 H), 7.91 (d, J = 4.4 Hz, 8 H, pyridine-H), 8.10-8.13 (m, 4 H, benzothiophene-H), 8.58-8.64 (m, 8 H, pyridine-H). ^{31}P NMR (CD_2Cl_2, 161.9 MHz, ppm): δ 12.98, 13.01 ($J_{Pt\text{-}P}$ = 2654.8 Hz). MS (ESI-MS): *m/z* calcd for [*p*-[**2**+**2**] - 3OTf$^-$]$^{3+}$ 1171.59, found 1171.67; [*p*-[**2**+**2**] - 2OTf$^-$]$^{2+}$ 1831.87, found 1831.95.

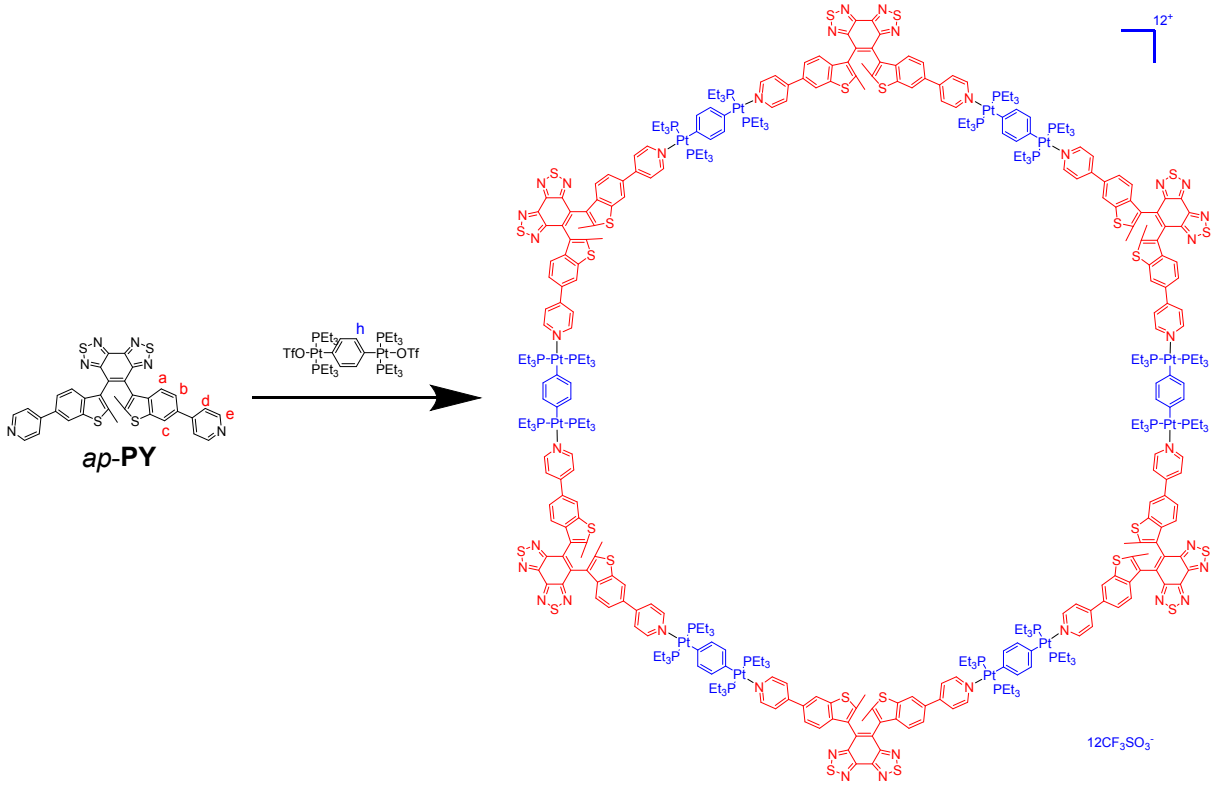

Scheme S2 Self-assembly of supramolecular hexagon *ap*-**[6+6]** from anti-parallel conformer ligand *ap*-**PY** and di-platinum acceptor **1**

Synthesis of *ap*-[6+6] hexagon: The dipyridyl donor ligand *ap*-**PY** (2.27 mg, 3.54 μmol) and the 180° acceptor **2** (4.38 mg, 3.54 μmol) were added to separate glass vials. To the vials containing the donor was added 0.2 mL of CD_2Cl_2, and the resulting solution was transferred to the acceptor vial charged with 0.2 mL of CD_2Cl_2. This process was repeated thrice with acetone-d_6 (3 × 0.15 mL) to ensure quantitative transfer of the donor to the acceptor. The reaction solution was then stirred at ambient temperature in dark for 5 h to yield a homogeneous light yellow solution. The solution was then transferred into the NMR tube to collect ^{1}H and ^{31}P NMR spectra. Light yellow solid product was obtained by removing the solvent under vacuum. Yield: 6.65 mg, > 99%. ^{1}H NMR (CD_2Cl_2 + acetone-d_6 , 400 MHz, ppm): δ 1.02-1.10 (m, 216 H, –PCH$_2$C**H$_3$**), 1.37-1.38 (m, 144 H, –PC**H$_2$**CH$_3$), 1.98 (s, 36 H, -CH$_3$), 7.05 (s, 24 H, phenyl-H), 7.51 (d, 12 H, J = 8.4 Hz, benzothiophene-H), 7.70 (d, 12 H, J = 8.4 Hz, benzothiophene-H), 8.05 (d, 12 H, J = 5.2 Hz, pyridine-H), 8.34 (s, 12 H, benzothiophene-H), 8.80 (d, 24 H, J = 5.2 Hz pyridine-H). ^{31}P NMR (CD_2Cl_2 + acetone-d_6, 161.9 MHz, ppm): δ 12.91 ($J_{Pt\text{-}P}$ = 2743.5 Hz). MS (ESI-MS): *m/z* calcd for [*ap*-[**6+6**] - 7OTf$^-$]$^{7+}$ 1460.30, found 1460.53.

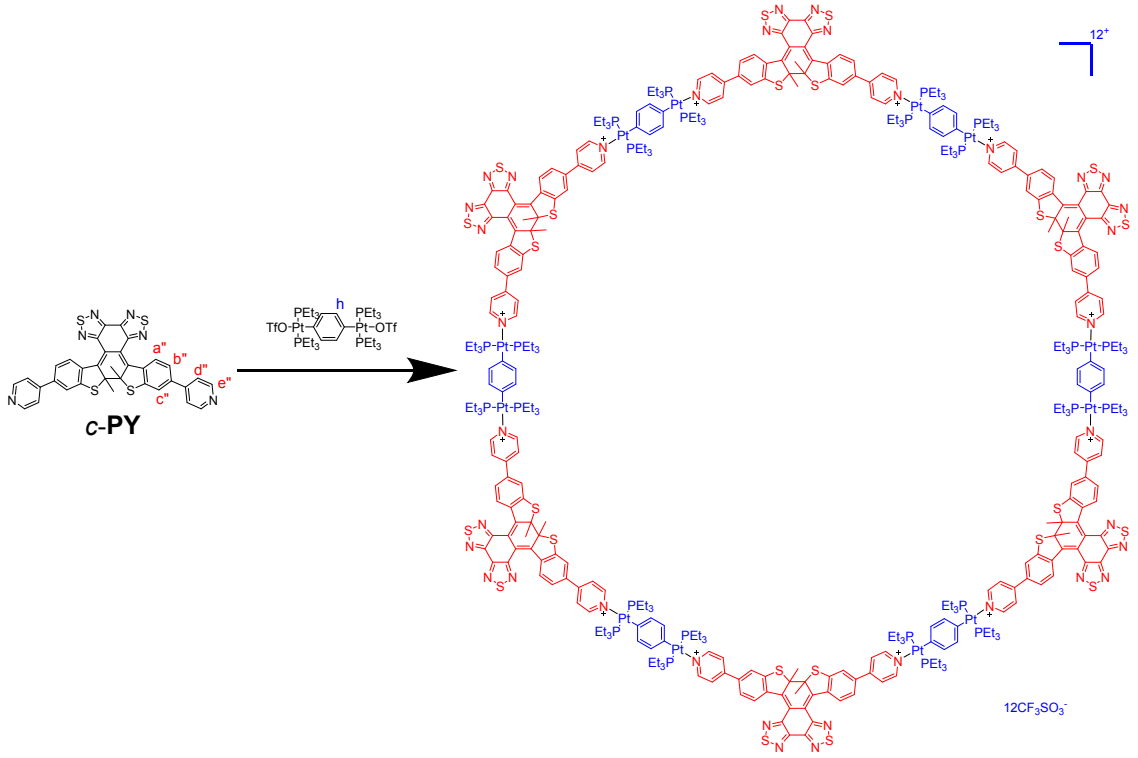

Scheme S3 Self-assembly of supramolecular hexagon *c*-**[6+6]** from anti-parallel conformer ligand *c*-**PY** and di-platinum acceptor **1**

Synthesis of *c*-[6+6] hexagon: The dipyridyl donor ligand *c*-**PY** (2.27 mg, 3.54 μmol) and the 180° acceptor **2** (4.38 mg, 3.54 μmol) were added to separate glass vials. To the vials containing the donor was added 0.2 mL of CD_2Cl_2, and the resulting solution was transferred to the acceptor vial charged with 0.2 mL of CD_2Cl_2. This process was repeated thrice with acetone-d_6 (3 × 0.15 mL) to ensure quantitative transfer of the donor to the acceptor. The reaction solution was then stirred at ambient temperature in dark for 5 h to yield a homogeneous dark red solution. The solution was then transferred into the NMR tube to collect ^{1}H and ^{31}P NMR spectra. Dark red solid product was obtained by removing the solvent under vacuum. Yield: 5.54 mg, > 99%. ^{1}H NMR (CD_2Cl_2 + acetone-d_6, 400 MHz, ppm): δ 1.05-1.08 (m, 216 H, –PCH$_2$C**H$_3$**), 1.33 (s, 144 H, –PC**H$_2$**CH$_3$), 2.02 (s, 36 H, -CH$_3$), 7.03 (s, 24 H, phenyl-H), 7.47 (d, 12 H, J = 7.6 Hz benzothiophene-H), 7.77 (s, 12 H, benzothiophene-H), 7.95 (s, 24 H, pyridine-H), 8.20 (d, 12 H, J = 7.6 Hz, benzothiophene-H), 8.75 (s, 24 H, pyridine-H). ^{31}P NMR (CD_2Cl_2 + acetone-d_6, 161.9 MHz, ppm): δ 12.94 ($J_{Pt\text{-}P}$ = 2736.1 Hz). MS (ESI-MS): *m/z* calcd for [*c*-**[6+6]** - 7OTf$^-$]$^{7+}$ 1460.0112, found: 1459.9688.

2. Chemical structure characterization

2.1 Chemical structure characterization of *p*-metallacycles

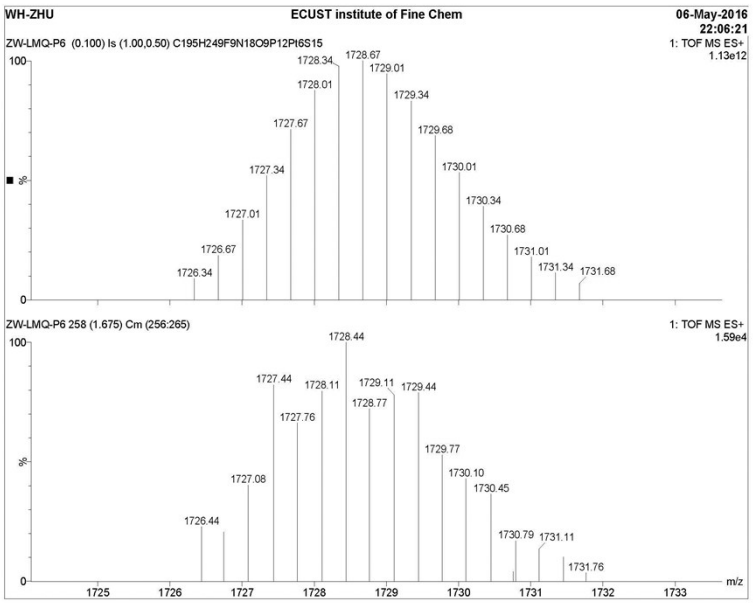

Fig. S1 Theoretical (top) and experimental (bottom) ESI-TOF-MS results of *p*-**[3+3]** of $[M\text{-}3OTf]^{3+}$

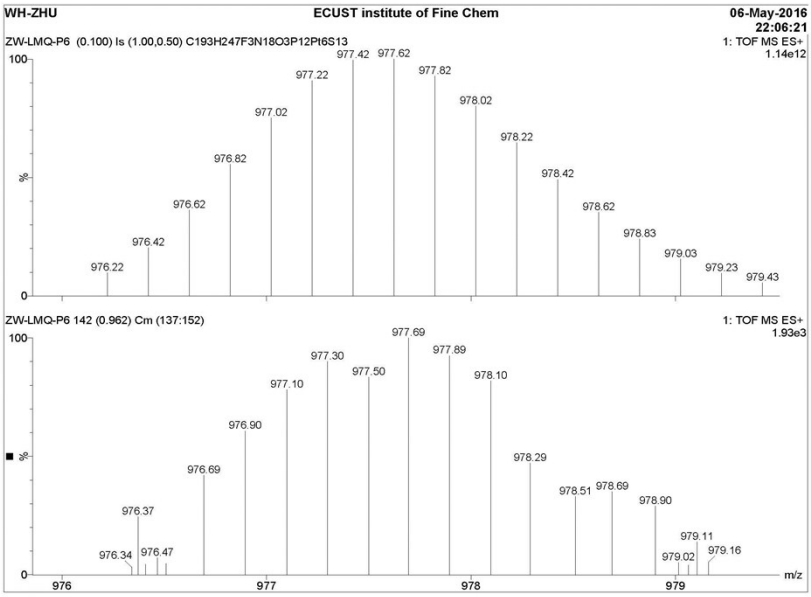

Fig. S2 Theoretical (top) and experimental (bottom) ESI-TOF-MS results of *p*-**[3+3]** of $[M\text{-}5OTf]^{5+}$

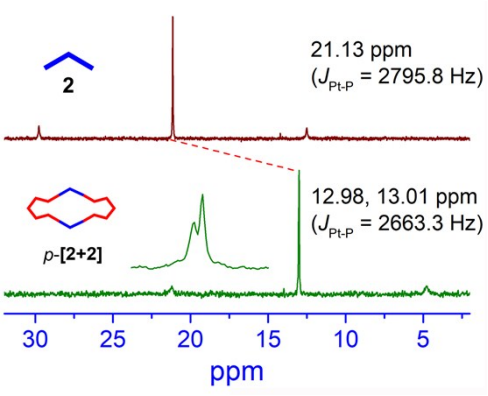

Fig. S3 The ^{31}P NMR spectra (161.9 MHz, CD_2Cl_2, 293 K) of 120° di-Pt(II) acceptor **2** and *p*-**[2+2]**.

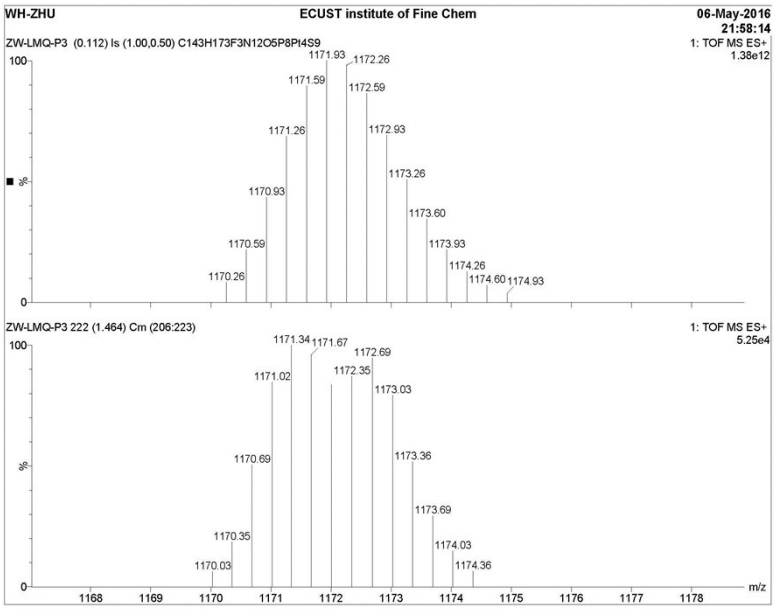

Fig. S4 Theoretical (top) and experimental (bottom) ESI-TOF-MS results of *p*-**[2+2]** of $[M\text{-}3OTf]^{3+}$

2.2 Chemical structure characterization of *ap*-metallacycles

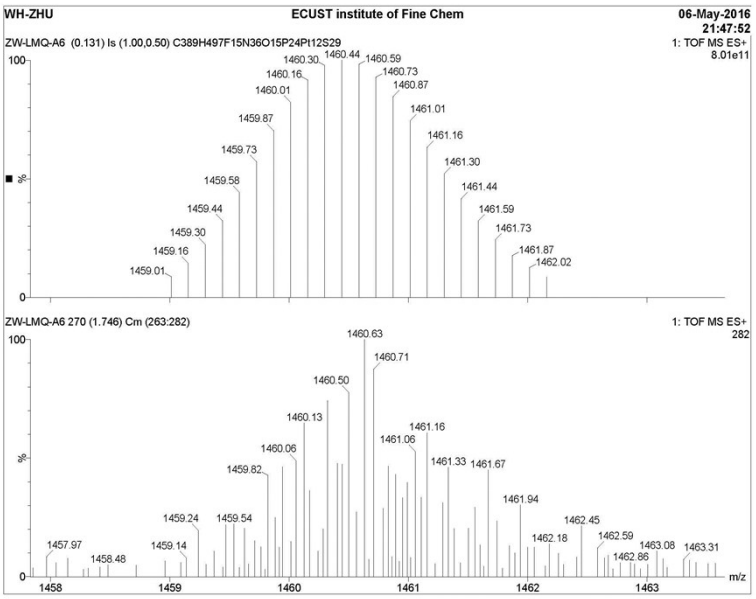

Fig. S5 Theoretical (top) and experimental (bottom) ESI-TOF-MS results of *ap*-**[6+6]** of $[M\text{-}7OTf]^{7+}$ (Note: The additional lines in *ap*-**[6+6]** might come from the signals of unknown fragments)

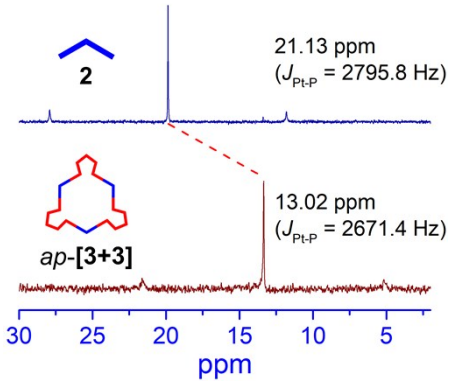

Fig. S6 ^{31}P NMR spectra (161.9 MHz, CD_2Cl_2, 293 K) of 120° di-Pt(II) acceptor **2** and *ap*-**[3+3]**.

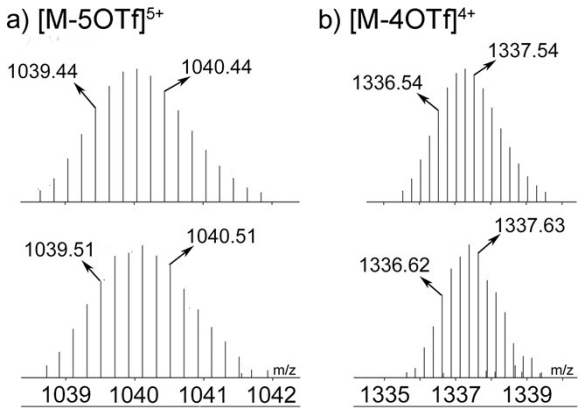

Fig. S7 Theoretical (top) and experimental (bottom) ESI-TOF-MS results of *ap*-**[3+3]** of (a) $[M\text{-}5OTf]^{5+}$ and (b) $[M\text{-}4OTf]^{4+}$

3 Chemical structure characterization of *c*-metallacycles

3.1 Partial ^{1}H NMR spectra of *c*-metallacycles

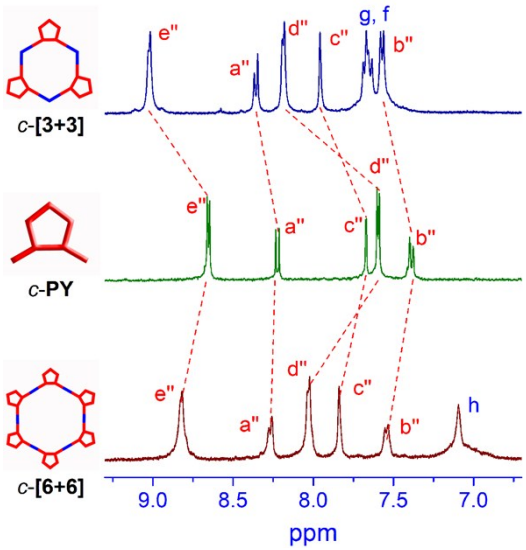

Fig. S8 Partial ^{1}H NMR spectra (400 MHz, 293 K) of *c*-**[3+3]**, *c*-**PY** and *c*-**[6+6]** in CD_2Cl_2 and acetone-d_6

3.2 Partial ^{31}P NMR spectra of *c*-metallacycles

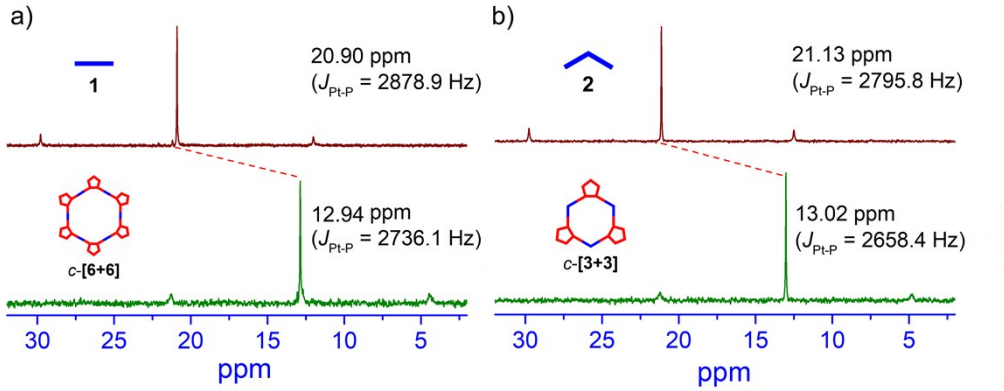

Fig. S9 ^{31}P NMR spectra (161.9 MHz, CD_2Cl_2, 293 K) of (**a**) 180° di-Pt(II) acceptor **1** and *c*-**[6+6]**, (b) 120° di-Pt(II) acceptor **2** and *c*-**[3+3]**.

3.3 ESI-TOF-MS of *c*-metallacycles

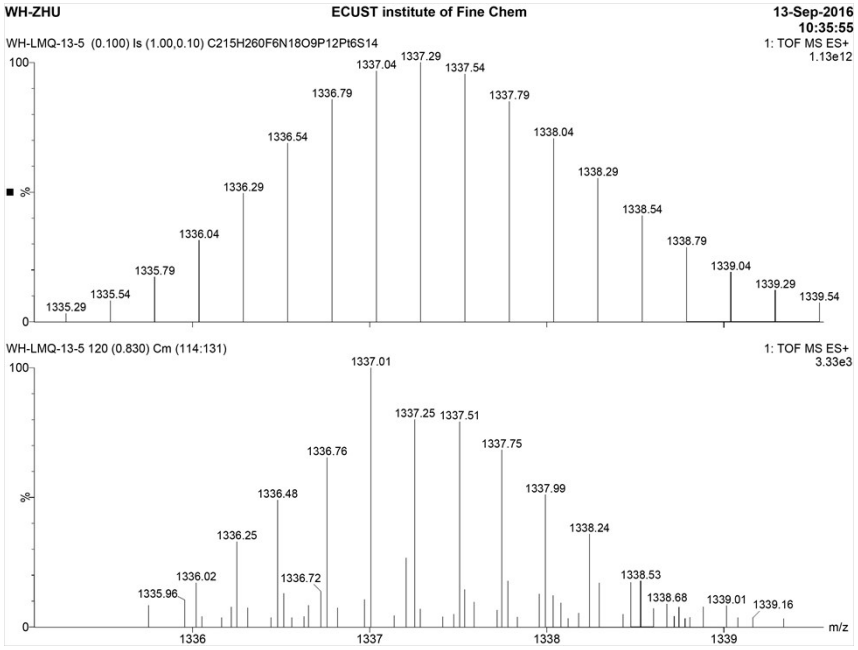

Fig. S10 Theoretical (top) and experimental (bottom) ESI-TOF-MS results of *c*-**[3+3]** of $[M\text{-}4OTf]^{4+}$

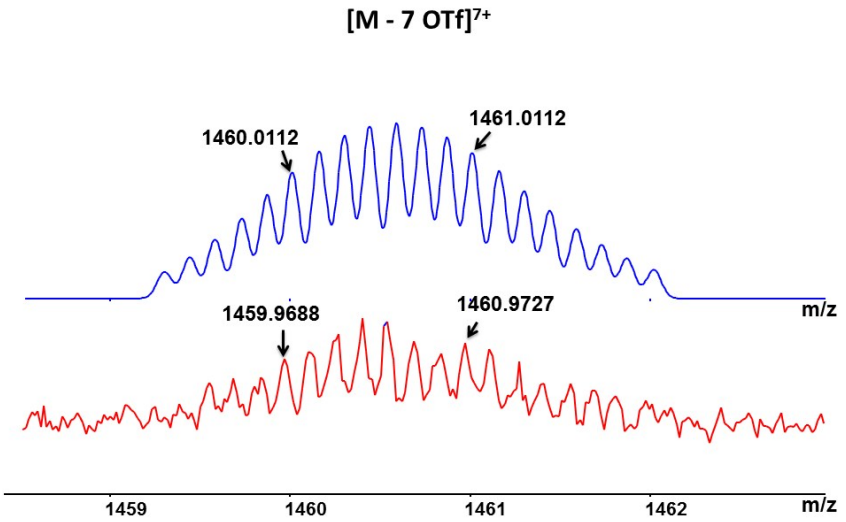

Fig. S11 Theoretical (top) and experimental (bottom) ESI-TOF-MS results of *c*-**[6+6]** of $[M\text{-}7OTf]^{7+}$

3.4 DOSY results of *c*-metallacycles

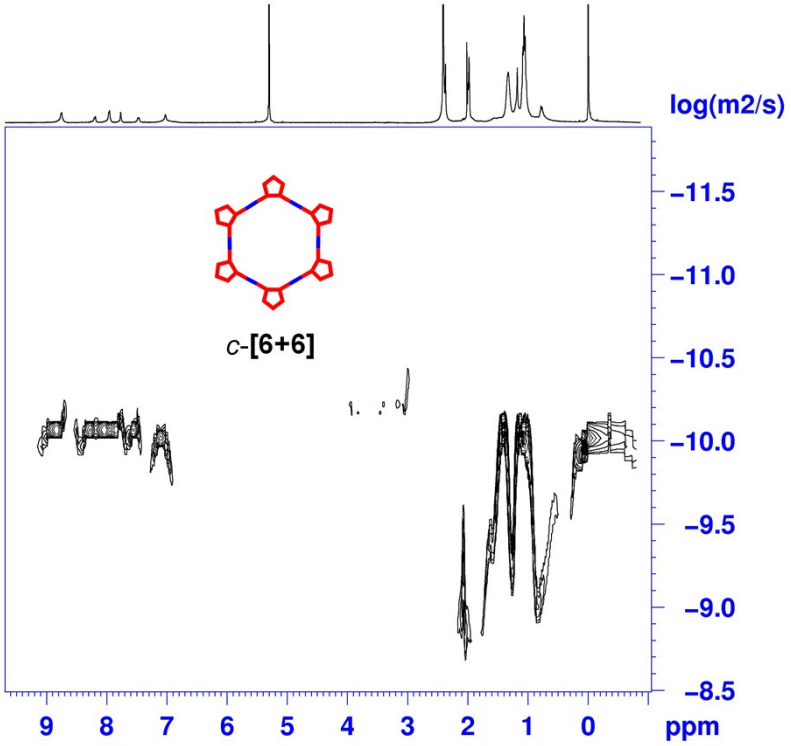

Fig. S12 2D DOSY (400 MHz, CD_2Cl_2 + acetone-d_6, 293 K) spectrum of *c*-**[6+6]**

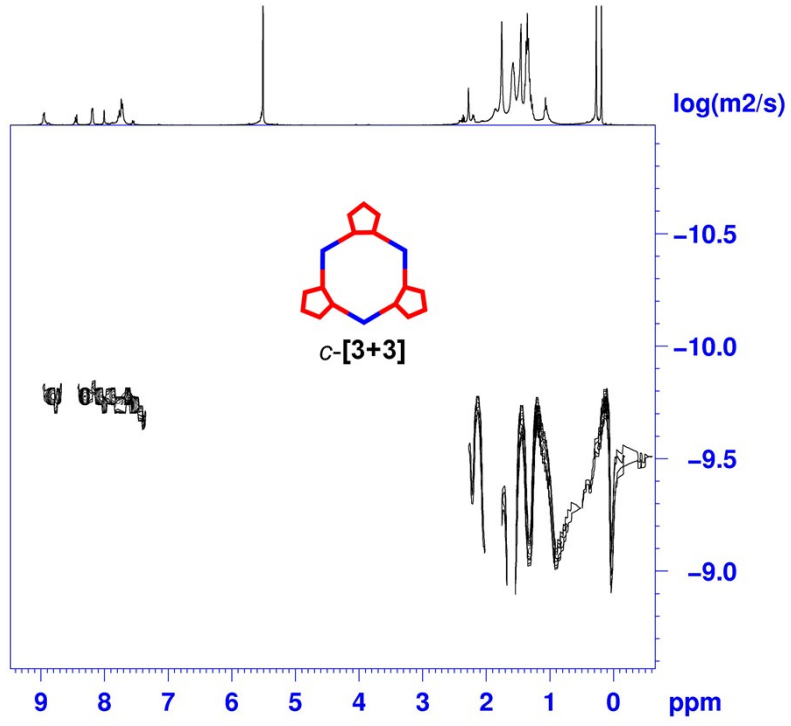

Fig. S13 2D DOSY (400 MHz, CD_2Cl_2 + acetone-d_6, 293 K) spectrum of *c*-**[3+3]**

4. Self-sorting behavior among *ap*-, *p*- and *c*-conformers

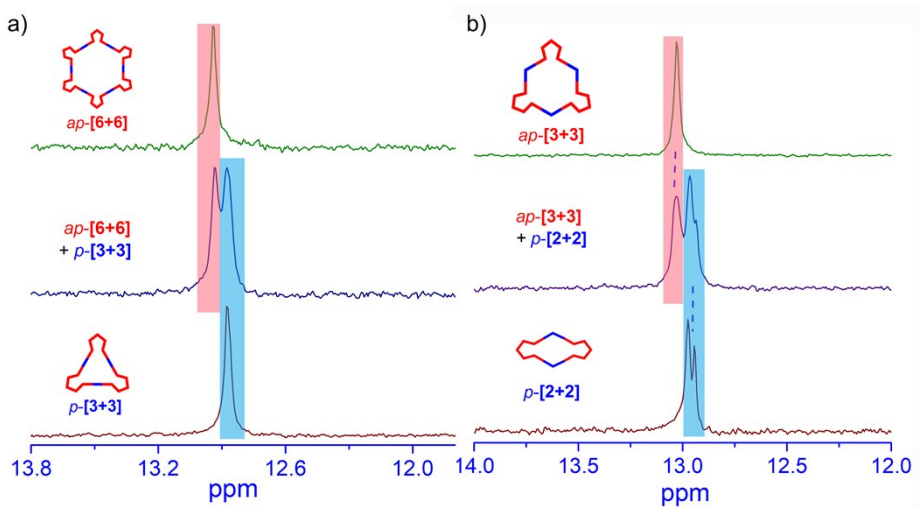

Fig. S14 Partial ^{31}P NMR spectra (161.9 MHz, CD_2Cl_2, 293 K) of (a) a*p*-**[6+6]**, mixed assembly systems and *p*-**[3+3]** in CD_2Cl_2 and DMSO-d_6; (b) a*p*-**[3+3]**, mixed assembly systems and *p*-**[2+2]** in CD_2Cl_2 and methanol-d_4.

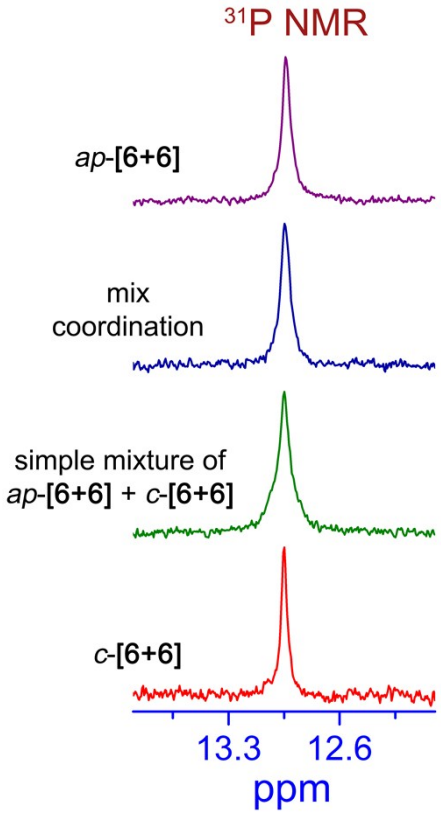

Fig. S15 Partial ^{31}P NMR (161.9 MHz, CD_2Cl_2 and DMSO-d_6, 293 K) spectra comparison of (a) *ap*-**[6+6]**, (b) mix coordination of 2.0 eq *ap*-**PY** and 1.0 eq *c*-**PY** with 3.0 eq Pt(Ⅱ) acceptor **1**, (c) *ap*-**[6+6]** + *c*-**[6+6]** (about 2: 1), (d) *c*-**[6+6]**.

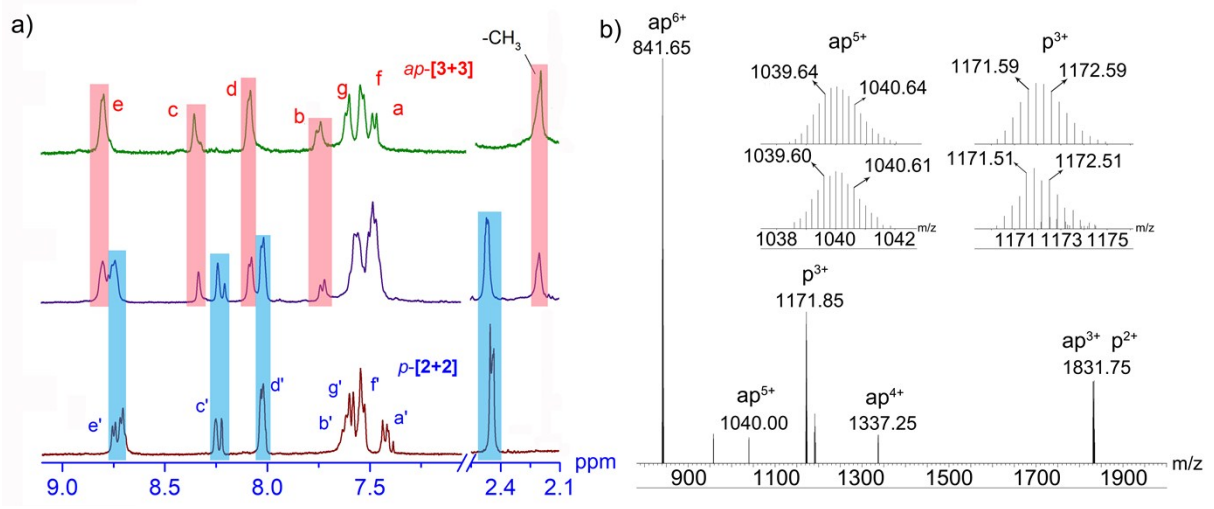

Fig. S16 Characterization of complex assembled by *ap*-PY and *p*-PY with di-Pt(II) **2**. (a) Partial ^{1}H NMR spectral comparison (400 MHz, 293 K) of a*p*-**[3+3]**, *p*-**[2+2]**, and mixed assembly systems in CD_2Cl_2. (b) ESI-TOF-MS results in the mixed assembly system of *ap*-**PY** and *p*-**PY** with di-Pt(II) **2**. Insets shows detailed ESI-TOF-MS peaks of *ap*-**[3+3]** of $[M\text{-}2OTf]^{2+}$ and *p*-**[2+2]** of $[M\text{-}3OTf]^{3+}$ (theoretical (top) and experimental (bottom)).

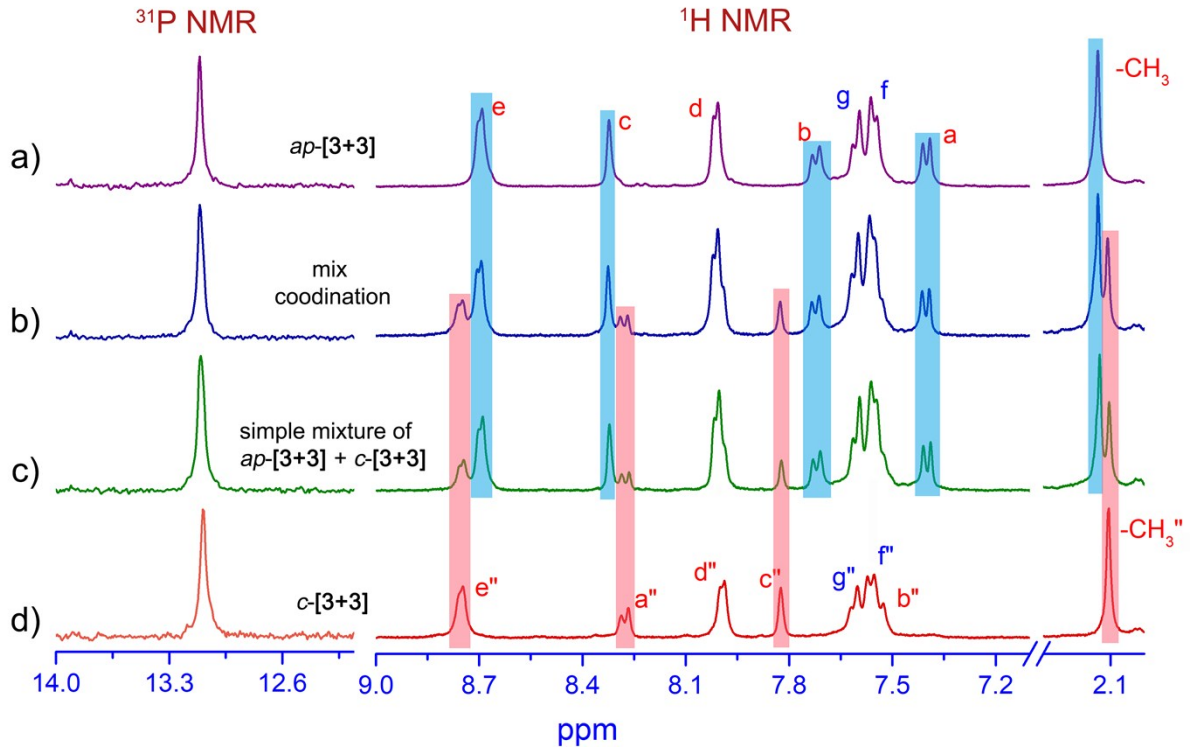

Fig. S17 Partial ^{1}H NMR (400 MHz, CD_2Cl_2 and Methanol-d_4, 293 K) and ^{31}P NMR (161.9 MHz, CD_2Cl_2 and Methanol-d_4, 293 K) spectra comparison of (a) *ap*-**[3+3]**, (b) mix coordination of 2.0 eq *ap*-**PY** and 1.0 eq *c*-**PY** with 3.0 eq Pt(Ⅱ) acceptor, (c) *ap*-**[3+3]** + *c*-**[3+3]** (about 2 :1) , (d) *c*-**[3+3]**.

5. Quantum chemical calculation

To further investigate the structure of the photochromic metallacycles, we tried to grow single crystal but none of them were suitable for X-ray analysis. Therefore, molecular simulation using the Gaussian 09[6] program package and optimized by semi-empirical PM6 calculations[7] was conducted to illustrate the structural characteristics of photoreponse metallacycles. Different from previous work of our groups, the shapes of *ap*- and *c*- metallacycles are similar to circle not hexagon due to larger bend angles between two pyridines. For *p*-conformer based metallacycles, the structure of matallacycles are assumed as above. The simulated structure of rhombiod *p*-**[2+2]** possesses a well-defined rhombus. Similarly, molecular simulation showed a roughly triangular structure for *p*-**[3+3]** (Fig. S18-S20). These results confirm the proper assembly of discrete and perfect structure of metallacycles again.

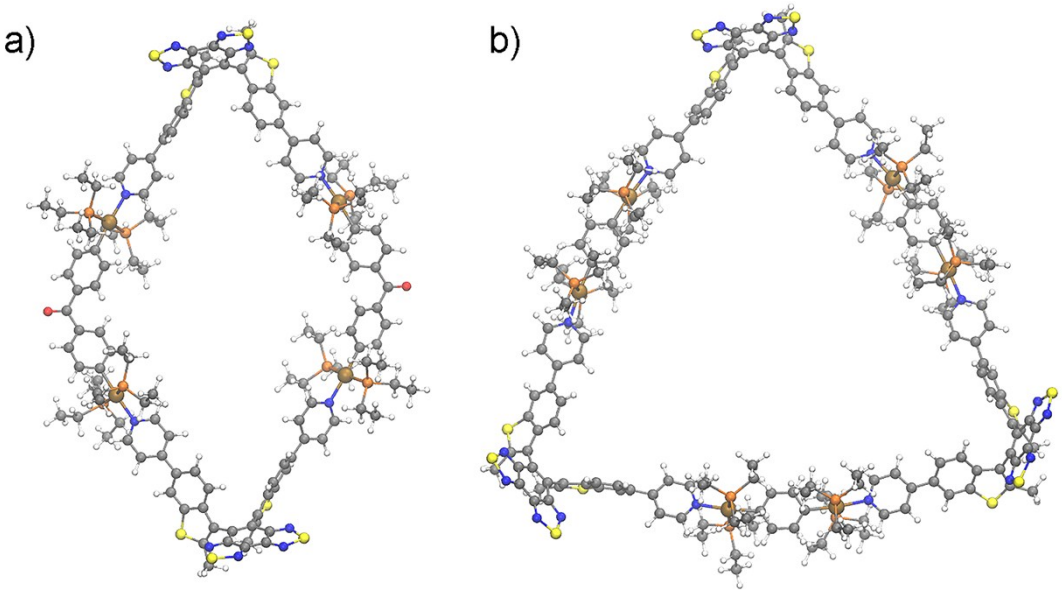

Fig. S18 Simulated molecular models (a) *p*-**[2+2]** and (b) *p*-**[3+3]** optimized by semi-empirical PM6 calculations, using the Gaussian 09 program package.

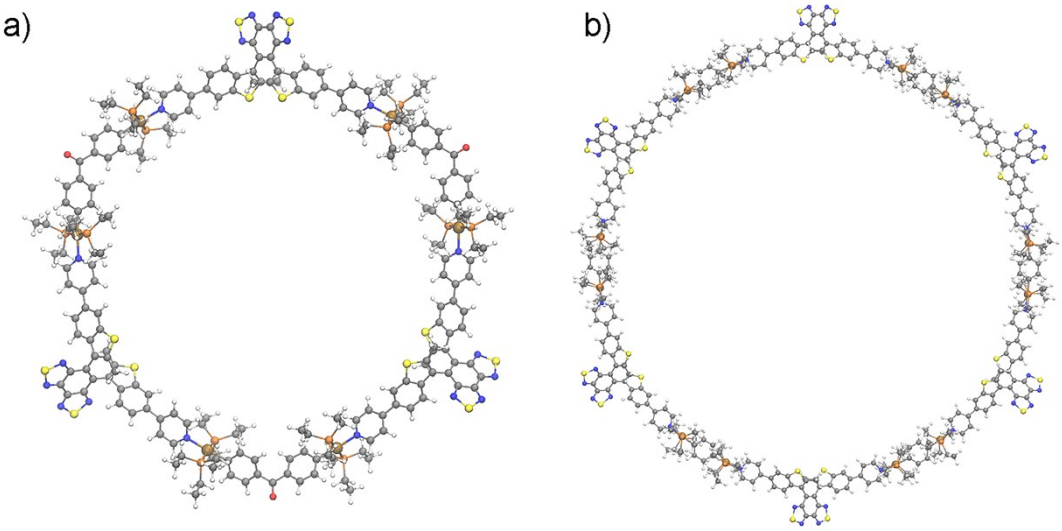

Fig. S19 Simulated molecular models (a) *ap*-**[3+3]** and (b) *ap*-**[6+6]** optimized by semi-empirical PM6 calculations, using the Gaussian 09 program package.

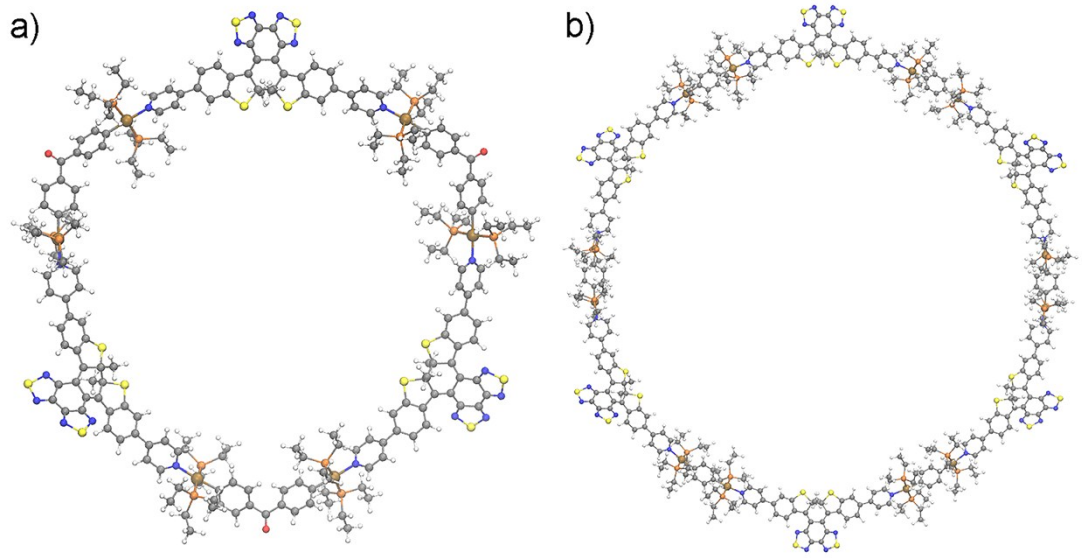

Fig. S20 Simulated molecular models a) *c*-**[3+3]** and b) *c*-**[6+6]** optimized by semi-empirical PM6 calculations, using the Gaussian 09 program package.

6. Photoresponse properties of ligand and metallacycles

6.1. Absorption and fluorescence changes of *p*-conformers

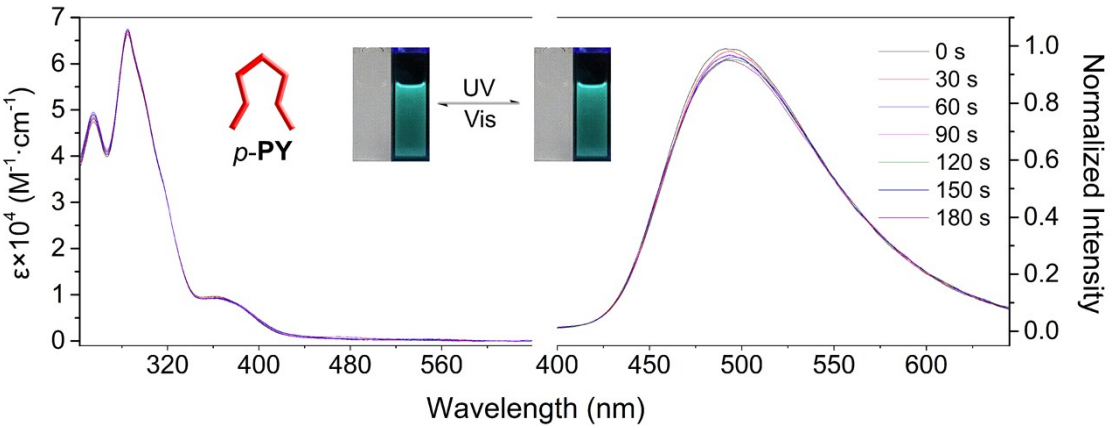

Fig. S21 Absorption and fluorescence change of *p*-**PY** in CH_2Cl_2 solution upon UV irradiation at 302 nm. Excitation for fluorescence is set at 331 nm. Inset images show the color and emission changes triggered by UV (λ = 302 nm) and Vis (λ > 480 nm) light.

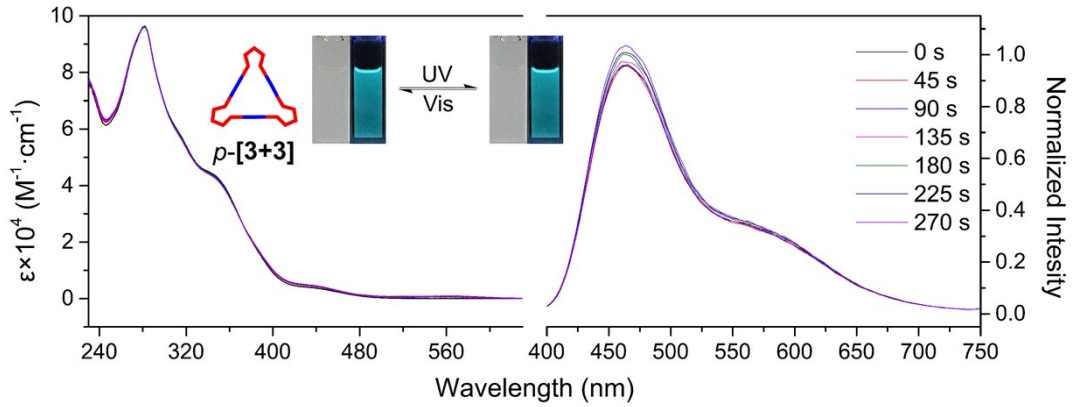

Fig. S22 Absorption and fluorescence changes of *p*-**[3+3]** in CH_2Cl_2 solution upon UV irradiation at 302 nm. Excitation for fluorescence is set at 375 nm. Inset images show the color and emission changes triggered by UV (λ = 302 ± 20 nm) and Vis (λ > 480 nm) light.

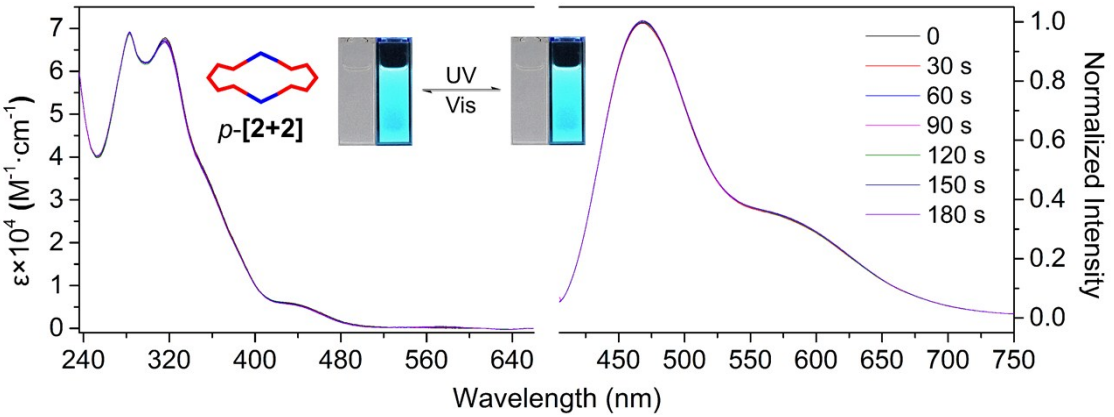

Fig. S23 Absorption and fluorescence changes of *p*-**[2+2]** in CH_2Cl_2 solution upon UV irradiation at 302 nm. Excitation for fluorescence is set at 376 nm. Inset images show the color and emission changes triggered by UV (λ = 302 ± 20 nm) and Vis (λ > 480 nm) light.

6.2. Photo-reversible response properties of *ap*-PY

For *ap*-conformer, upon irradiation at 302 nm light, the CH_2Cl_2 solution turned red, along with forming a series of peaks located at 384, 420 and 549 nm, ascribing to the formation of *c*-**PY**, which is resulted from the typical photocyclization. The conversion ratio of photocyclization is calculated to be 94.3% when reaching the photostationary state (PSS) (Fig. 7a). Moreover, the fluorescence of *ap*-**PY** shows a blue light located at 519 nm upon excitation at the isosbestic point of 331 nm. At the same time, the fluorescence was quenched with open form transforming to closed form by 94.8% due to the formation of non-fluorescence *c*-**PY** (Fig. 7a). We also tested the photocyclization and cycloreversion quantum yields of *ap*-**PY**. $\Phi_{o\text{-}c}$ and $\Phi_{c\text{-}o}$ of *ap*-**PY** in CH_2Cl_2 solution were determined about 73.4% and 4.6%, respectively (Table 1).

Moreover, the color of PSS of *ap*-**PY** can be completely bleached by visible light (λ > 480 nm) as a result of photocycloreversion. When later irradiated by 302 nm light, the color turned red again and the spectra turn similar to *c*-**PY**. Furthermore, this compound can be repeatedly irradiated by UV (302 nm) and visible light (λ > 480 nm) alternatively for 12 times without any obvious degradation, indicative of excellent fatigue resistance (Fig. S36a).

6.3 Photo-reversible response properties of *ap*-[3+3]

Metallacycle trimer *ap*-**[3+3]** also exhibited excellent photo-responsive performance which has been reported previously. Upon UV light irradiation (302 ± 20 nm), the solution color turned from colorless to red with an increase at visible light region which attributed to the formation of ring-closed metallacycle *c*-**[3+3]** through a typical photocyclization process. When reaching PSS, the conversion ratio was about 93% (Fig. S24). Also, several photo-switching cycles were performed showing excellent fatigue resistance without any obvious degradation (Fig. S36c).

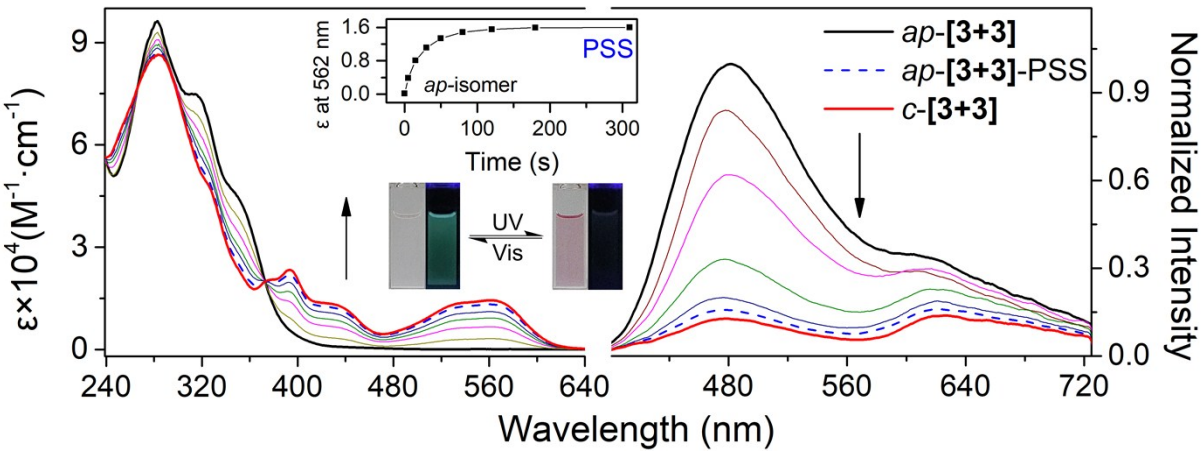

Fig. S24 Light induced spectral change of *ap*-**[3+3]**. Absorption and fluorescence spectra of *ap*-**[3+3]**, respectively, under irradiation of UV light (λ = 302 ± 10 nm) in CH_2Cl_2. Excitation for fluorescence is set at each isobestic point. Inset images show the color and emission changes triggered by UV (λ = 302 ± 20 nm) and Vis (λ > 480 nm) light and the inset spectral changes of extinction coefficient

7. Conformer comparison on optical properties

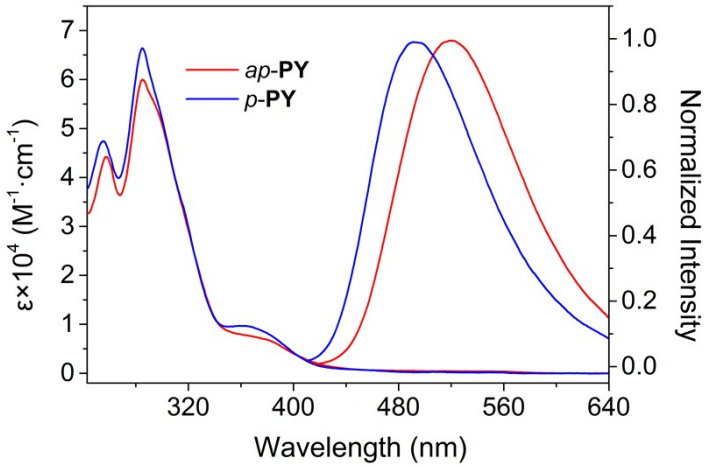

Fig. S25 Contrast of absorption and fluorescence of *ap*-**PY** and *p*-**PY** in CH_2Cl_2 solution. The excitation of fluorescence is set at 331 nm.

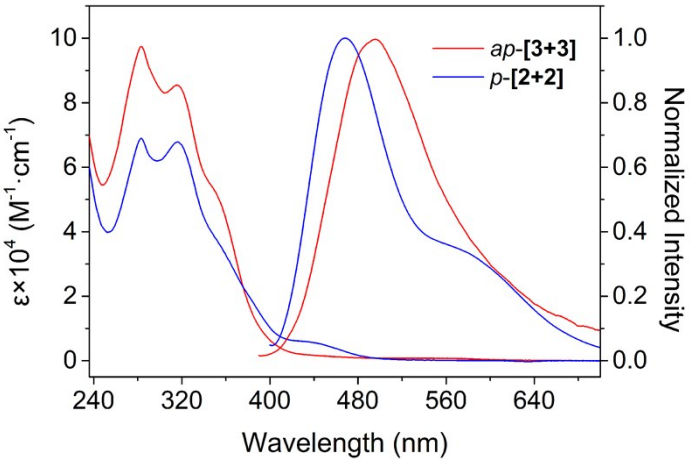

Fig. S26 Contrast of absorption and fluorescence of *ap*-**[3+3]** and *p*-**[2+2]** in CH_2Cl_2 solution. The excitation of fluorescence is set at 376 nm.

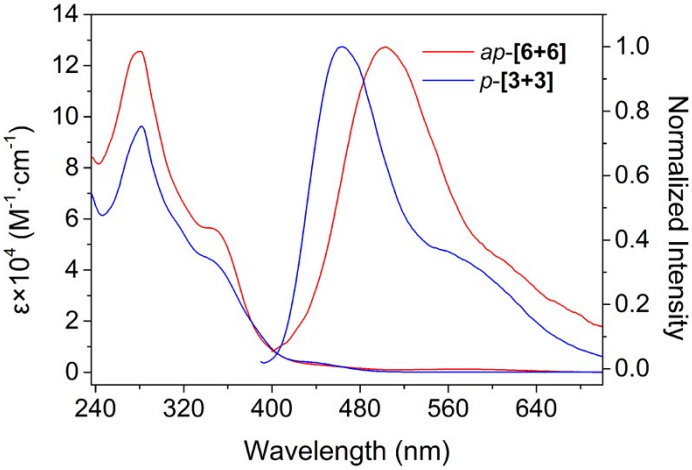

Fig. S27 Contrast of absorption and fluorescence of *ap*-**[6+6]** and *p*-**[3+3]** in CH_2Cl_2 solution. The excitation of fluorescence is set at 375 nm.

We compared the optical properties of *ap*- and *p*- conformer.

(1) First, we compared optical properties of *ap*-**PY** and *p*-**PY**. Their absorption are almost the same except that the absorption of *p*-**PY** are slightly stronger than *ap*-**PY**. They both show weak fluorescence resulting from the ICT due to typical D-π-A structure. Meanwhile the emission peak of *ap*-**PY** is red-shifted by 24 nm compared to *p*-**PY** (Fig. S25).

(2) Next, we compared the optical properties of *ap*- and *p*- conformers of metallacycles. Upon coordinated to the same Pt salts, *ap*- conformers always shows higher absorption coefficients than *p*-conformers. For instance, *ap*-**[6+6]** shows a strong peaks at 280 nm with molar extinction coefficients of 124.5×10^3 $M^{-1} \cdot cm^{-1}$ based on each photochromic units, while molar coefficient extinction of *p*-**[3+3]** at 281 nm is only about 96.2×10^3 $M^{-1} \cdot cm^{-1}$. Another pair of metallacycles also shows the similar results. This phenomenon may be related to the size of the metallacycles that there are more photoresponsive units, it shows higher molar extinction coefficients (Fig. S26-S27).

(3) Compared with *ap*-conformer, all the emission peaks of *p*-conformer metallacycles show blue-shift. For example, the fluorescence peaks of *p*-**[3+3]** located at 464 nm which is blue-shifted by 39 nm compared to *ap*-**[6+6]**.

8. Comparison of optical properties between ligands and metallacycles in CH_2Cl_2 solution

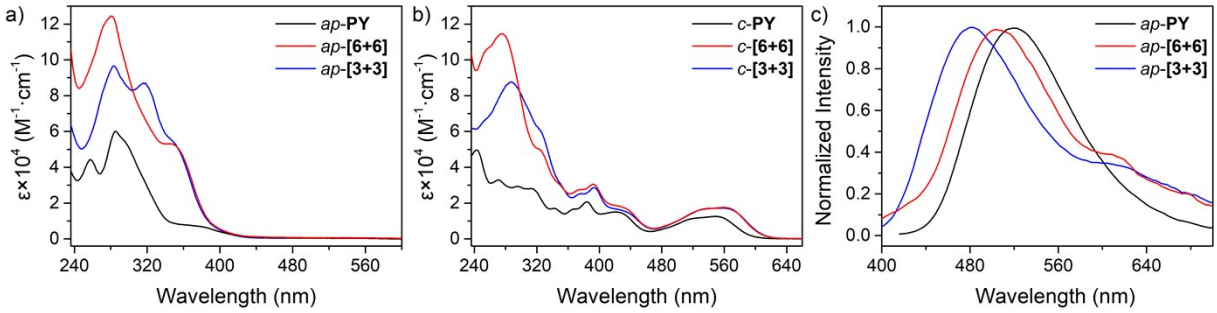

Fig. S28 Spectra comparison of ligand and metallacycles of *ap*-conformer and *c*-isomer. (a) Absorption spectra comparison between *ap*-**PY** ($c = 2.10 \times 10^{-5}$ M), *ap*-**[6+6]** ($c = 2.13 \times 10^{-6}$ M) and *ap*-**[3+3]** ($c = 4.47 \times 10^{-6}$ M) which the molar extinction coefficients of metallacycles are calculated by concentration of photoresponse unit; (b) Absorption spectra *c*-**PY,** *c*-**[6+6]** and *c*-**[3+3]** which the molar extinction coefficients of metallacycles are calculated by concentration of photoresponse unit; (c) Normalized emission spectra of *ap*-**PY**, *ap*-**[6+6]** and *ap*-**[3+3]**.

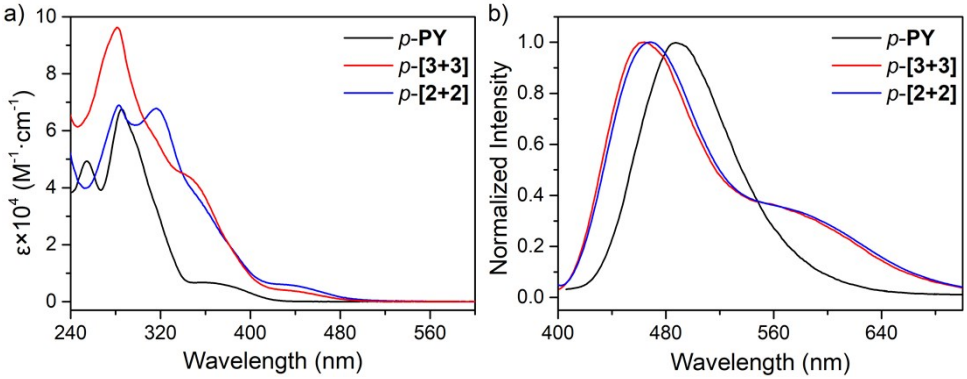

Fig. S29 Spectra comparison of ligand and metallacycles of *p*-conformer. (a) Absorption spectra comparison between *p*-**PY** ($c = 2.18 \times 10^{-5}$ M), *p*-**[3+3]** ($c = 3.31 \times 10^{-6}$ M) and *p*-**[2+2]** ($c = 5.68 \times 10^{-6}$ M) which the molar extinction coefficient of metallacycles are calculated by concentration of *p*-**PY**; (b) Normalized emission spectra of *p*-**PY**, *p*-**[3+3]** and *p*-**[2+2].**

We compared the absorption spectra between non-assembled conformer building blocks and resulting metallacycles. From the spectra, it could be found quite large differences.

(1) The open metallacycle (*ap*-**[6+6])** contains six photochromic units, exhibiting a strong absorbance band

at 280 nm with molar absorbance coefficients of 747.0 × 10^3 M^{-1}·cm^{-1}, that is, 124.5 × 10^3 M^{-1}·cm^{-1} for each photochromic units. The molar coefficient extinction of ligands in open form (*ap*-**PY)** at 285 nm is only about 59.9 × 10^3 M^{-1}·cm^{-1}. Compared with the absorption spectra in the open form, the assembled compounds (*ap*-**[6+6]**) exhibited a higher intensity of absorbance coefficients based on each photochromic unit which means it would be more sensitive to photo than *ap*-**PY** which can enhance the sensitivity of supramolecular. Similar phenomenon can also be found in *ap*-**[3+3]** (Fig. S28a).

(2) With regard to closed-ring isomers, similarly, closed metallacycle (*c*-**[6+6]**) contains six closed photoresponse units, showing a strong band at 559 nm with molar absorbance coefficients of 109.2 × 10^3 M^{-1}·cm^{-1}, that is, 18.2 × 10^3 M^{-1}·cm^{-1} for each photochromic units. The molar coefficient extinction of ligands in closed form (*c*-**PY)** at 549 nm is only about 12.6 × 10^3 M^{-1}·cm^{-1}. Compared with the absorption spectra in the closed form, the assembled compounds (*c*-**[6+6]**) exhibited a higher intensity of absorbance extinction coefficients based on each photochromic unit and a red-shift by 10 nm compared to *c*-**PY** (Table 1). The results also means it would be more sensitive to photons than *c*-**PY** (Fig. S28b).

(3) As for parallel conformer, the similar intensity enhancement can also be observed in *p*-**[3+3]**. It contains three parallel conformer units, showing a strong band at 281 nm with the molar absorbance coefficients of 288.6 × 10^3 M^{-1}·cm^{-1}, that is, 96.2 × 10^3 M^{-1}·cm^{-1} for each photochromic units. The molar extinction coefficient of ligands in closed form (*p*-**PY)** at 285 nm is only about 66.4 × 10^3 M^{-1}·cm^{-1}. Compared with the absorption spectra in the parallel isomer, the assembled compounds (*p*-**[3+3]**) exhibited a higher intensity of absorbance extinction coefficients based on each photochromic unit (Fig. S29a).

However, for *p*-**[2+2]**, it contais two parallel conformer units, showing a band with molar absorbance coefficients of 137.8 × 10^3 M^{-1}·cm^{-1} at 283 nm, that is 68.9 × 10^3 M^{-1}·cm^{-1} for each photochromic units. Compared with unassembled ligand, it shows similar intensity based on each photochromic unit.

Moreover, compared to free ligands, there appears a new shoulder peaks at 410-490 nm for both parallel conformer metallacycles may be attributed to the extended π conjugation upon coordination of *p*-**PY** with Pt acceptors.

(3) There appears a new peak at 314 nm in the absorption spectra for both *ap*-**[3+3]** and *p*-**[2+2]** which can be ascribed to di-platinum(Ⅱ) acceptor **2**.

(4) After assemble to Pt(Ⅱ) acceptor, the emission peak displays a quite large blue-shifted for all the metallacycles along with a decrease in fluorescence quantum yields. This phenomenon can be attributed to weakness of donor due to coordination. It also shows an unexpected emission peak related to the coordination bond in the self-assembled metallacycle (Fig. S28c and S29b).

9. Study on phototransformation process of *ap*-metalllacycles

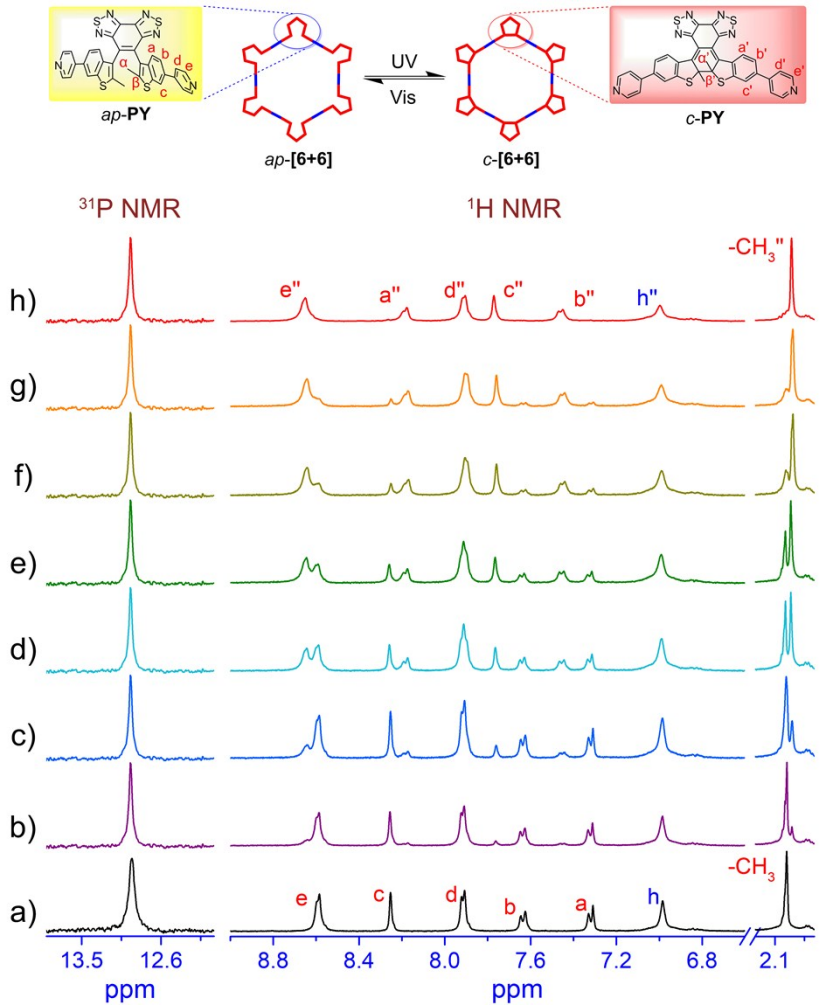

Fig. S30 ^{1}H NMR spectra of structural transformation of *ap*-**[6+6]** from ring-open to ring-closed form (CD_2Cl_2, 293 K): (a) *ap*-**[6+6]**; (b) upon irradiation at 302 nm for 5 min; (c) 30 min; (d) 75 min; (e) 100 min; f) 160 min, g) 280 min, h) *c*-**[6+6]**. Note: it is necessary to take a long time irradiation to reach PSS due to the high concentration of the sample (ca. 1.5×10^{-3} M) during monitoring NMR spectral changes.

10. Fluorescence study of metallacycles

10.1 Fluorescence lifetime of ligand and metallacycles

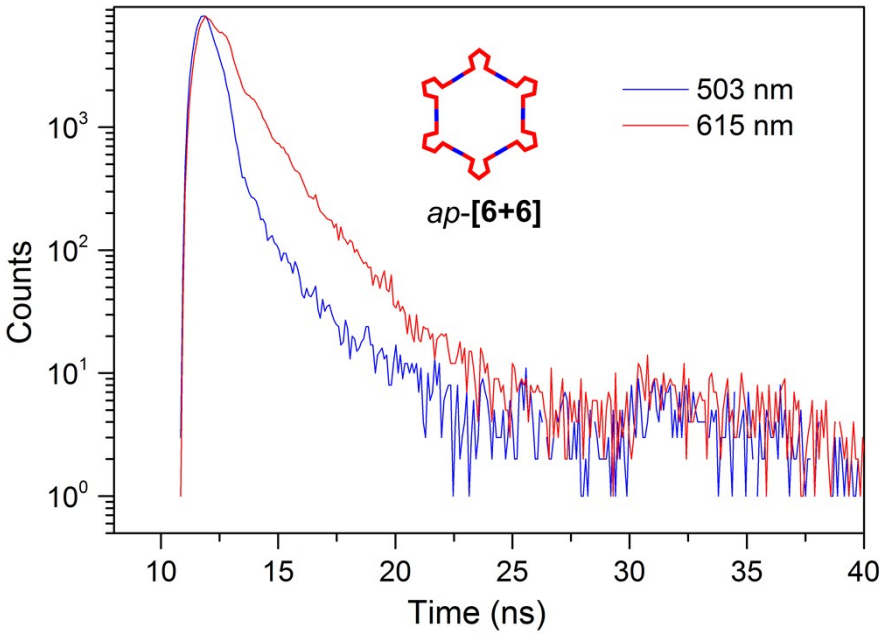

Fig. S31 Flurescence decay of *ap*-**[6+6]** in DCM solutions at different wavelength

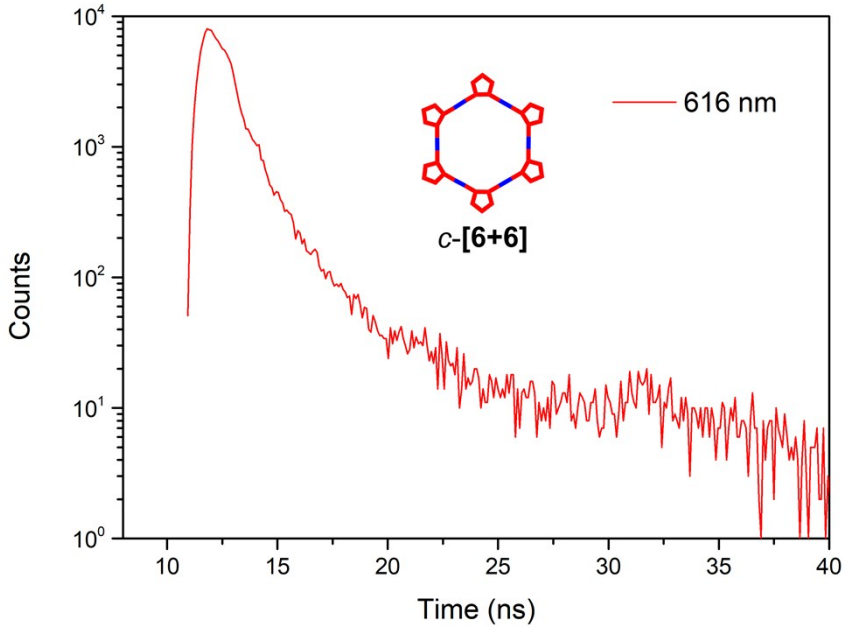

Fig. S32 Fluorescence decay of *c*-**[6+6]** in DCM solutions

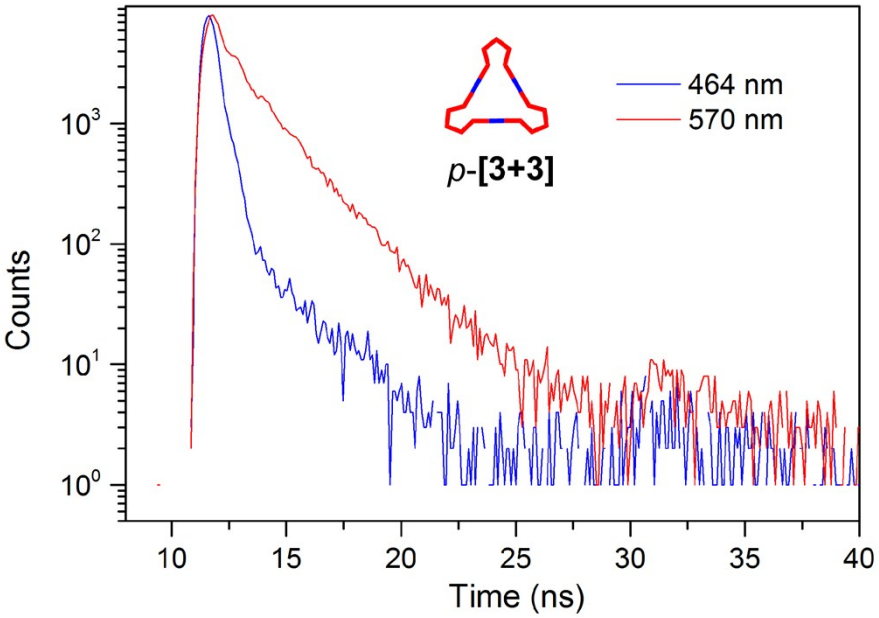

Fig. S33 Fluorescence decay of *p*-**[3+3]** in DCM solutions at different wavelength

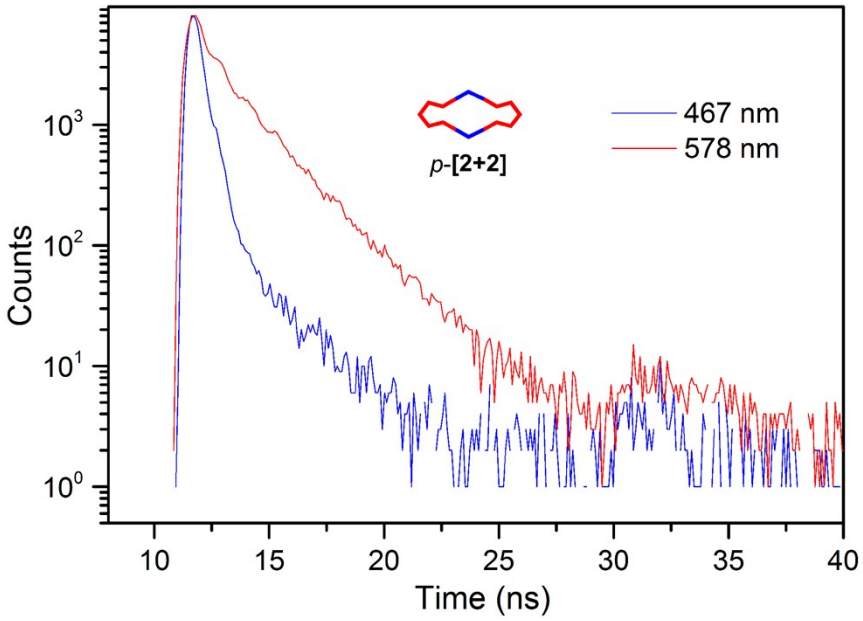

Fig. S34 Fluorescence decay of *p*-**[2+2]** in DCM solutions at different wavelength

10.2. Absorption and fluorescence changes of *ap*-PH with acceptor 1

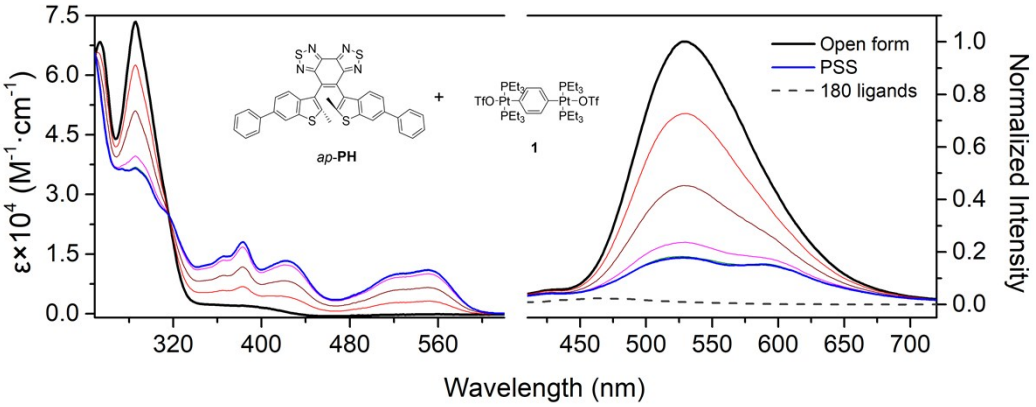

Fig. S35 Absorption and fluorescence changes of *ap*-**PH** + 180° ligands in DCM solutions upon UV irradiation at 302 nm. Excitation for fluorescence is set at 374 nm.

11. Photoreversible properties of *ap*-ligands and *ap*-metallacycles

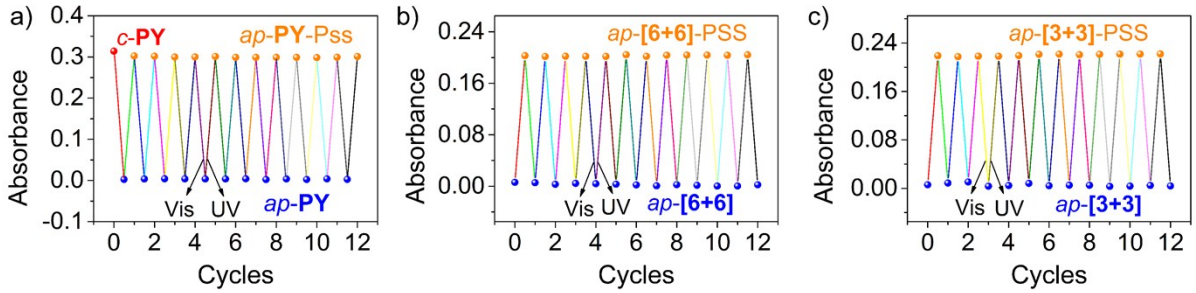

Fig. S36 (a) Absorption *ap*-**PY** (λ=549 nm, c = 2.51×10^{-5} M), (b) *ap*-**[6+6]** (λ=559 nm, c = 1.90×10^{-6} M) and (c) *ap*-**[3+3]** (λ=562 nm, c =3.97×10^{-6} M) in DCM solution upon irradiation of UV light (λ = 302 nm) and visible light (λ>480 nm), alternatively.

12. Single Crystal data

X-ray crystallographic data can be obtained free of charge from the Cambridge Crystallographic Data Center (www.ccdc.cam.ac.uk/data_request/cif) under accession numbers CCDC: 1848524 (*p*-**PY**).

Table S1 Crystal and structure determinations data of *p*-**PY**

compounds	*p*-**PY**
Empirical formula	C34 H20.25 N6 O0.12 S4
Formula weight	643.05
Temperature / K	100(2)
Wavelength / Å	1.54178
Crystal system	Orthorhombic
Space group	P b c n
a / Å	32.3746(6)
b / Å	8.0807(2)
c / Å	22.6746(6)
α / deg	90
β / deg	90
c / deg	90
Volume / $Å^3$	5931.9(2)
Z	8
Density (calculated) / Mg/m^3	1.440
Absorption coefficient / mm^{-1}	3.240
F(000)	2650
Crystal size / mm^3	0.240 × 0.150 × 0.060
Theta range for data collection / deg	3.899 to 73.260
Index ranges	-39<=h<=40, -9<=k<=7, -27<=l<=27
Reflections collected	17184
Independent reflections	5795 [R(int) = 0.0325]
Max. and min. transmission	1.00000 and 0.69049
Data / restraints / parameters	5795 / 0 / 402
Goodness-of-fit on F2	1.025
Final R indices [I>2sigma(I)]	R1 = 0.0537, wR2 = 0.1425
R indices (all data)	R1 = 0.0716, wR2 = 0.1550
Largest diff. peak and hole / $e.Å^{-3}$	0.753 and -0.482

13. Characterization

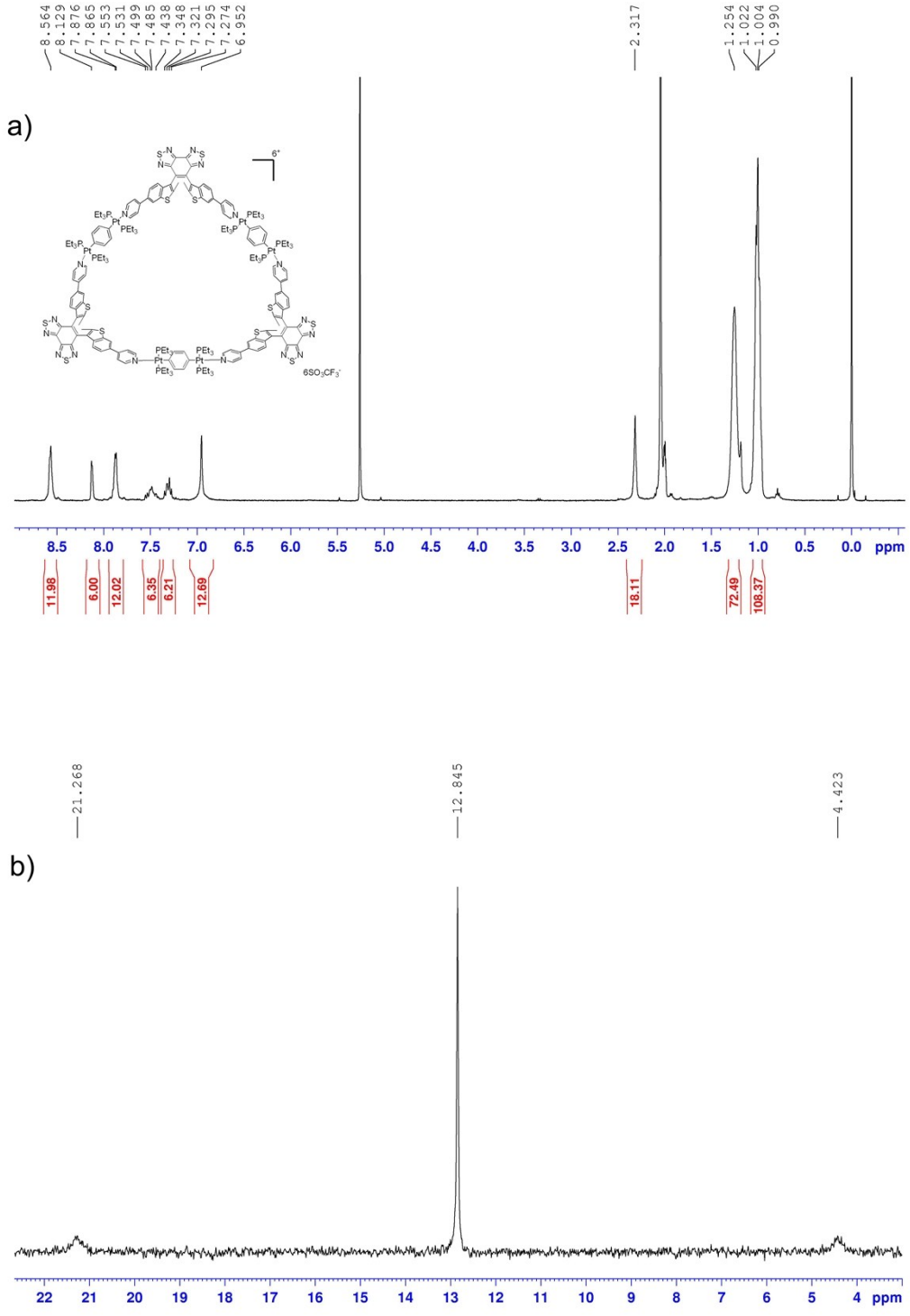

Fig. S37 (a) ^{1}H NMR spectrum (400 MHz, CD_2Cl_2, 293 K) and (b) ^{31}P NMR spectrum (161.9 MHz, CD_2Cl_2, 293 K) of ***p*-[3+3]**

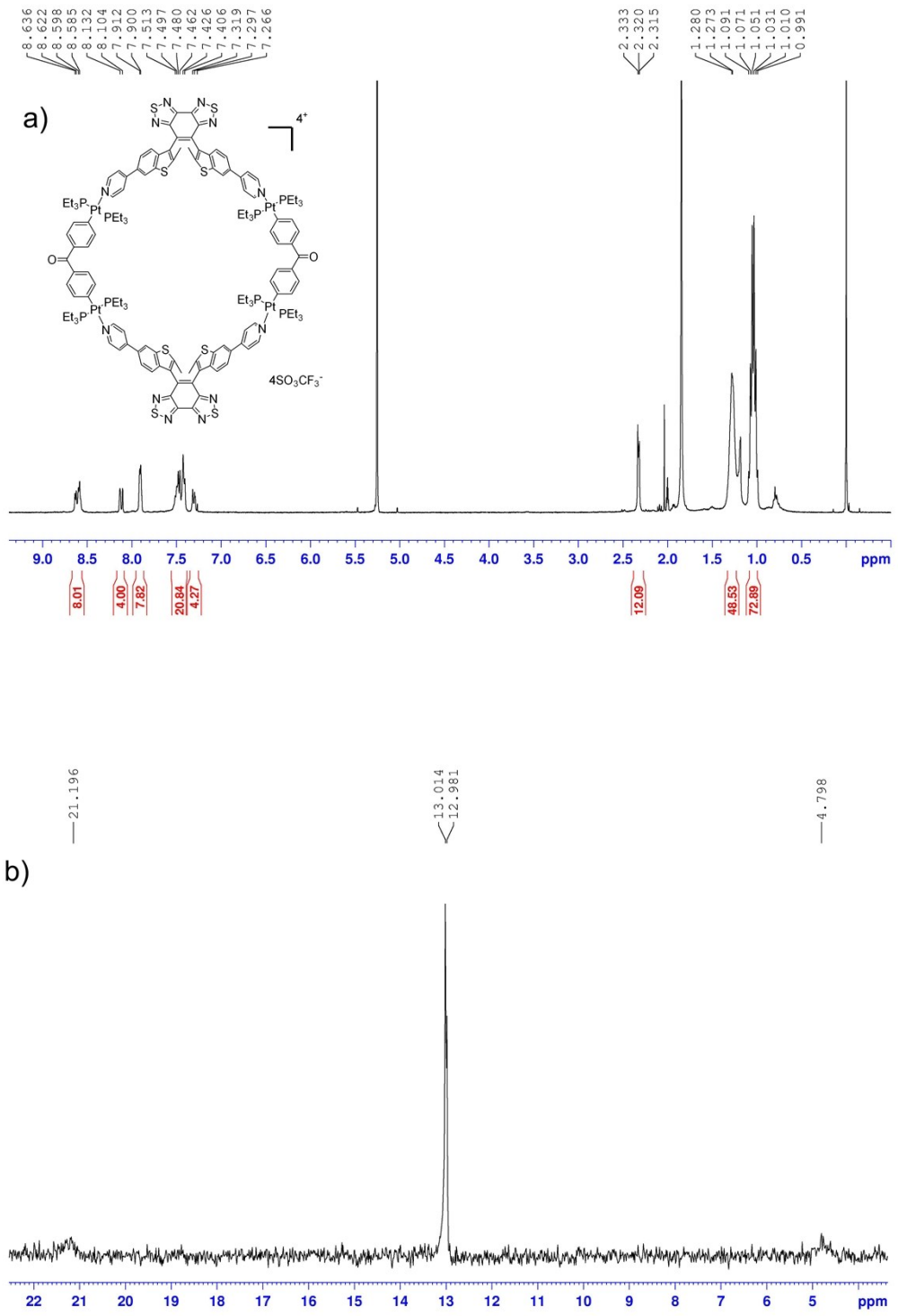

Fig. S38 (a) ^{1}H NMR spectrum (400 MHz, CD_2Cl_2, 293 K) and (b) ^{31}P NMR spectrum (161.9 MHz, CD_2Cl_2, 293 K) of ***p*-[2+2]**

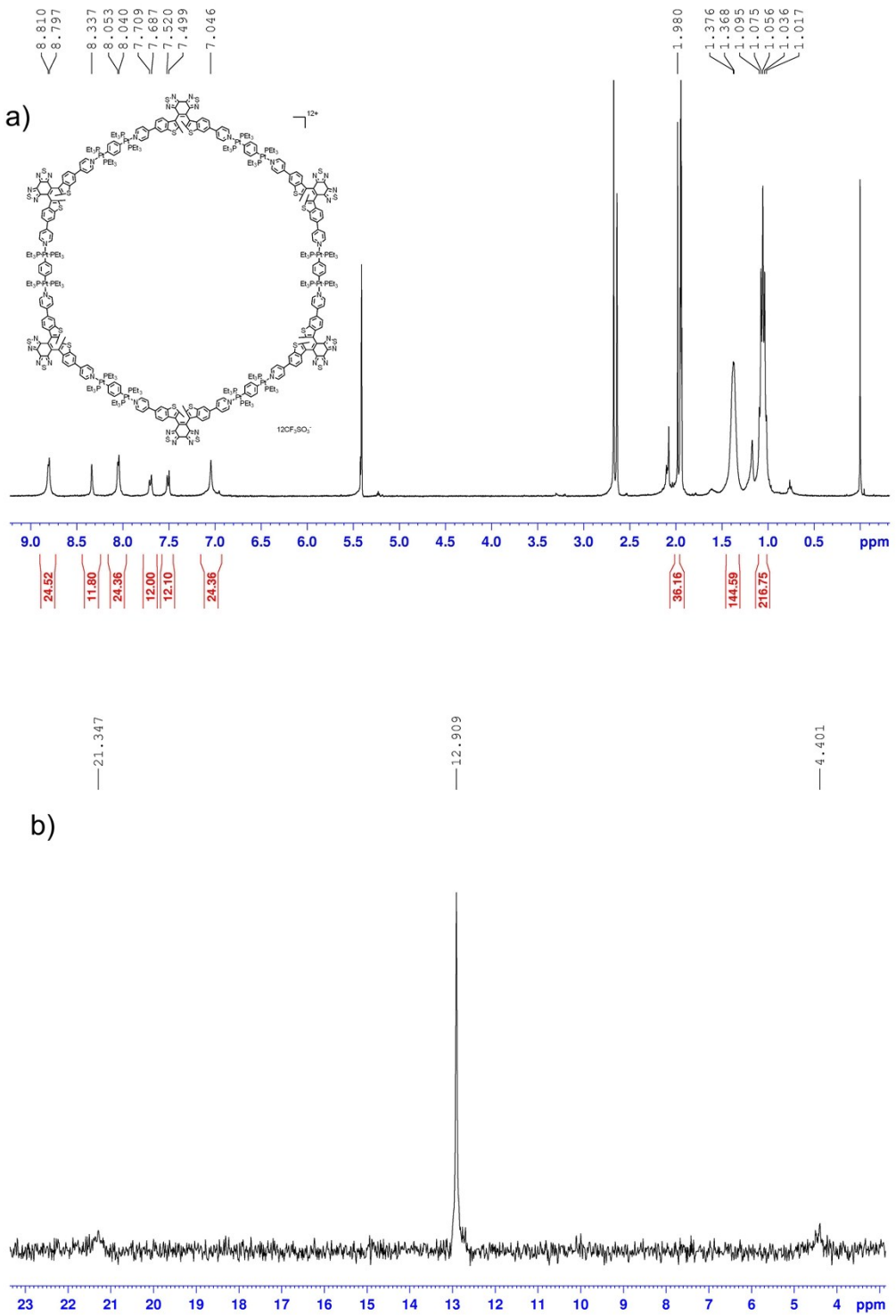

Fig. S39 (a) ^{1}H NMR spectrum (400 MHz, CD_2Cl_2 + acetone-d_6, 293 K) of and (b) ^{31}P NMR spectrum (161.9 MHz, CD_2Cl_2 + acetone-d_6, 293 K) of *ap*-**[6+6]**

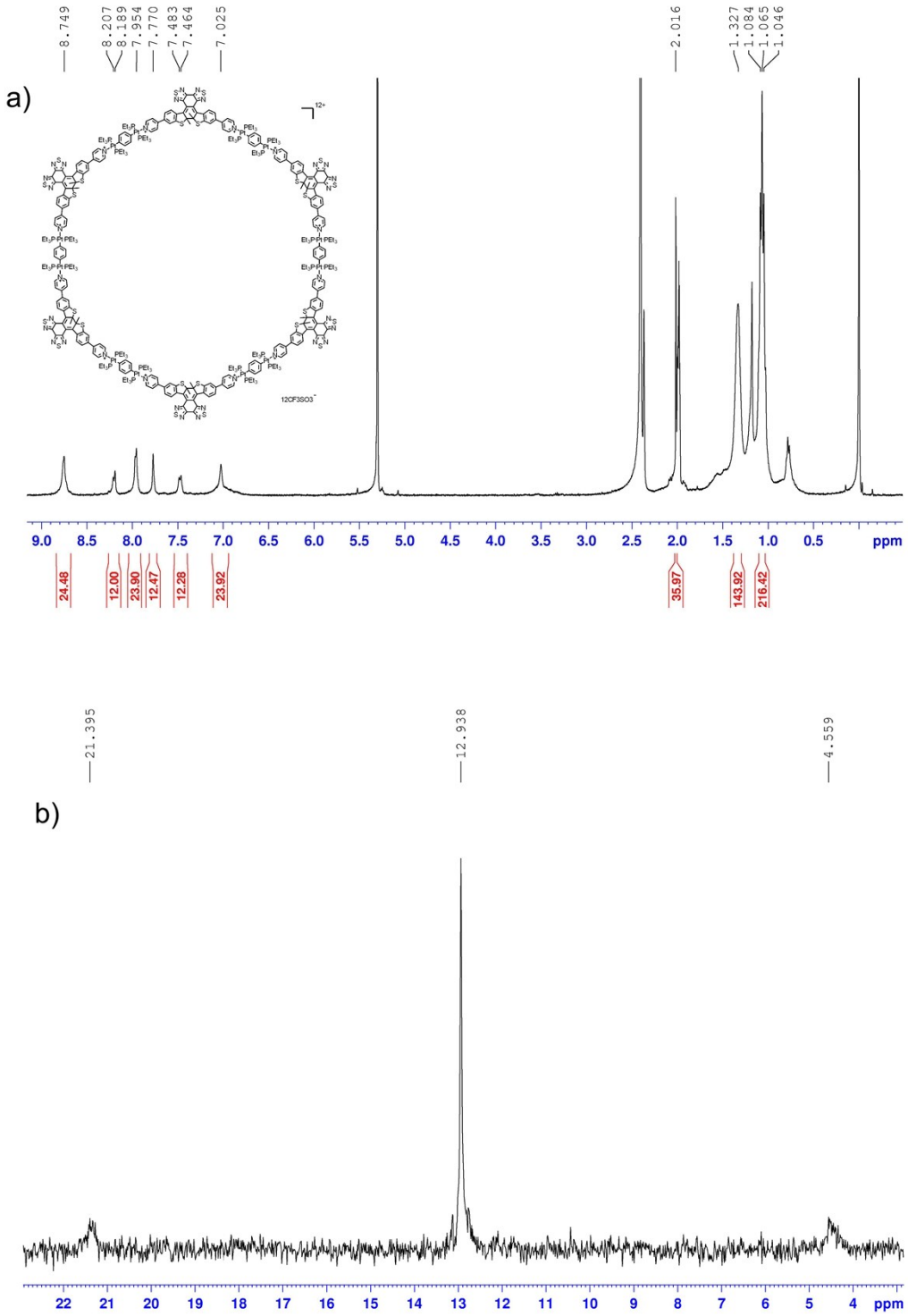

Fig. S40 (a) ^{1}H NMR spectrum (400 MHz, CD_2Cl_2 + acetone-d_6, 293 K) and (b) ^{31}P NMR spectrum (161.9 MHz, CD_2Cl_2 + acetone-d_6, 293 K) of *c*-**[6+6]**

References

1. M. Li, L.-J. Chen, Y. Cai, Q. Luo, W. Li, H.-B. Yang, H. Tian and W.-H. Zhu, *Chem*, 2019, **5**, 634.
2. S. Leininger, M. Schmitz and P. J. Stang, *Org. Lett.*, 1999, **1**, 1921.
3. J. Manna, C. J. Kuehl, J. A. Whiteford, P. J. Stang, D. C. Muddiman, S. A. Hofstadler and R. D. Smith, *J. Am. Chem. Soc.*, 1997, **119**, 11611.
4. S. Fukumoto, T. Nakashima and T. Kawai, *Angew. Chem.*, *Int. Ed.*, 2011, **50**, 1565.
5. W. Melhuish, *J. Phys. Chem.*, 1961, **65**, 229.
6. M. Frisch, G. Trucks, H. Schlegel, G. Scuseria, M. Robb, J. Cheeseman, G. Scalmani, V. Barone, B. Mennucci and G. Petersson, *Gaussian 09 Revision D. 01, 2009*, 2009.
7. J. J. Stewart, *J. Mol. Model.*, 2007, **13**, 1173.